Meccanica (2013) 48:1263–1287
DOI 10.1007/s11012-012-9666-7

Static analysis of multilayered smart shells subjected to mechanical, thermal and electrical loads

Salvatore Brischetto · Erasmo Carrera

Received: 11 April 2012 / Accepted: 9 November 2012 / Published online: 28 November 2012

Abstract The paper introduces a quasi-3D static description of multilayered smart shells subjected to mechanical, thermal and electrical loads and it evaluates the coupling between each physical field and the effects of the shell curvatures. The governing equations are solved in a closed form and they are given in terms of three main primary variables (displacement vector, temperature and electric potential). The displacements can be modelled in both Equivalent Single Layer (ESL) or Layer Wise (LW) form, the temperature and the electric potential are always considered in LW form because of their higher spatial gradients. Independently of the multilayer approach, each variable can be expanded from linear to fourth order in the thickness direction. Comparisons between these refined 2D models and the classical ones are also proposed to show the main advantages and limitations. The fully coupled thermo-electro-mechanical governing equations are obtained from opportune extensions of the Principle of Virtual Displacements and the multifield constitutive equations.

Part of this work has been presented at the XX Congresso AIMETA—Bologna, 12–15 September, 2011 with the title "S. Brischetto and E. Carrera. Thermo-electro-mechanical coupling in smart structures subjected to field loadings".

S. Brischetto (✉) · E. Carrera
Department of Mechanical and Aerospace Engineering, Politecnico di Torino, Corso Duca degli Abruzzi, 24, 10129 Torino, Italy
e-mail: salvatore.brischetto@polito.it

Keywords Coupling and curvature effects · Multifield loads · Multilayered smart shells · Refined models · Classical models · Thermo-electro-mechanical governing equations

1 Introduction

Smart structures can be defined as multilayered two-dimensional structures embedding homogeneous, composite and piezoelectric layers where the electric field can be used to counteract (actuator configuration) or to supervise (sensor configuration) thermo-mechanical deformations [1, 2]. The most common two-dimensional structures employed in aeronautic and space field are multilayered plates and shells, the static electro-thermo-mechanical analysis of multilayered plates has already been proposed in [3], this new work considers multilayered shell structures subjected to mechanical, thermal and electrical loads in order to also evaluate possible curvature effects. Smart shells give the possibility to analyze the coupling between three different physical fields. The main problems in multilayered structures are the interfaces, which lead to discontinuous distributions of thermal, electrical and mechanical properties along the thickness, and the presence of "field loadings" such as the electrical and thermal ones. The use of refined two-dimensional models could be mandatory to contrast such problems. Nowinski's book [4] suggests that the mechanical and thermal aspects are coupled and inseparable, and such a suggestion has been received in [5]

where the thermo-mechanical coupling has been analyzed in one-layered and multilayered shells by means of fully coupled thermo-mechanical governing equations where both displacements and temperature are primary variables.

The main topic of the present work is the extension of the Principle of Virtual Displacements (PVD) to thermo-electro-mechanical problems by the addition of the internal thermal and electrical works to the mechanical one, fully coupled thermo-electro-mechanical models can be obtained to analyze smart structures subjected to different loadings such as mechanical, electrical and thermal ones and to evaluate the weight and importance of the different coupling effects between the three physical fields involved. The electro-mechanical coupling of smart shells has already been proposed in past authors' works [6, 7], the addition of the thermal field introduces several complications (in particular in terms of thermo-mechanical and thermo-electrical couplings) which will be deeply discussed in the present paper. The PVD has been extended to the thermo-electro-mechanical case in accordance to the suggestions in Altay and Dökmeci [8] where both the constitutive equations and the variational statement are discussed, but no benchmarks are proposed. The most important features for the coupling between the thermal and mechanical fields are discussed in [9] and [10]. Luo et al. [11] have proposed the correct extension of the PVD to the thermo-electro-mechanical analysis by including the different multi-fields couplings. Constitutive and governing equations have also been given but they have not been solved, therefore no results, benchmarks and assessments have been proposed. A review of theoretical developments in thermopiezoelasticity, having relevance to smart composite structures, has been presented in [12]. The governing equations for the linear response of piezothermoelastic media have been outlined. Sensor applications have been used to predict thermal loads and corresponding responses from measurements of electric potential distributions; studies on the control of composite structures (beams, plates and shells) via piezoelectric actuation have been reviewed. However, a full coupling for the thermal field has not been considered in the works presented in such a revision [12]. El-Karamany [13] has obtained the constitutive laws for the linear thermopiezoelectric/piezomagnetic continuum, and the equations of motion by means of the extended Hamilton principle. A three-phase cylindrical model for fiber composites subjected to in-plane mechanical load under the coupling effects of multi-physical fields (thermal, electric, magnetic and elastic) has been presented in [14]. This three-phase model can also be applied to fiber/interphase/matrix composites where interesting thermo-electro-magnetism and stress coupling phenomena, induced by the interphase layer, have been revealed. This work demonstrates as the multifield analyses are also important for those problems different from the "classical" structural plate/shell analyses.

In recent years several works have proposed the thermo-electro-mechanical analysis of multilayered shells, the most significant ones are discussed in the following part. Dumir et al. [15] have given exact solutions for smart shells subjected to pressure and electrostatic loadings for various values of radius to thickness ratio, the full coupling between the electrical and mechanical fields has been considered. The results proposed could be used as reference solutions for such two-dimensional models developed for the analysis of shell structures where the thermal field effects and its coupling are not included. Dai and Wang [16] have presented an analytical solution for magneto-thermo-electro-elastic problems of a piezoelectric hollow cylinder placed in an axial magnetic field subjected to arbitrary thermal shock, mechanical load and transient electric excitation. From numerical results, it is clear how the model proposed allows the analysis for different multi-field loadings but a full coupling between the physical fields involved has not been introduced. A semi-analytical finite element formulation has been presented in [17] for the analysis of active controlled shells of revolution taking into account a steady state temperature field over the piezoelectric and elastic structural continuum. In general it has been found that there is a thermal deflection in dynamic oscillation and this thermal deflection is not the same for different axial modes. The results proposed are quite interesting even if a classical shell model such as the First order Shear Deformation Theory (FSDT) has been used for the elastic shells of revolution. An higher order zigzag shell theory based on general tensor formulation has been developed in [18] to refine the predictions of the mechanical, thermal and electric behaviors. In order to assess the validity of the theory proposed, the shell behavior has been evaluated under the thermal and electric loads as well as under the mechanical load. This theory is suitable for the prediction

of deformations and stresses in thick smart composite shells subjected to mechanical, thermal and electric loads, but no considerations have been proposed about the full coupling between the physical fields. Roy et al. [19] have developed an improved eight node finite element formulation for piezothermoelastic analysis of smart fiber reinforced polymer (FRP) composite shells with bonded piezoelectric sensors and actuators. The transverse shear effect has also been included in according to Mindlin's hypotheses. Pyroelectric effect has been considered in the formulation and it has a significant influence on the response of such shells under piezothermoelastic loading. Different types of smart shell panels have been analyzed and the coupled thermo-electro-mechanical responses have been presented. In [20], dynamic buckling of imperfect FGM cylindrical shells with integrated surface-bonded sensor and actuator layers subjected to some complex combinations of thermo-electro-mechanical loads has been investigated. Effects of temperature dependency of material properties, volume fraction index, load combination and initial geometric imperfections on thermo-electro-mechanical post-buckling behavior have been evaluated, the thermal field is not full coupled. Sheng and Wang [21] have proposed a shear deformation theory (FSDT) for an approximate solution for functionally graded laminated piezoelectric cylindrical shells under thermal shock and moving mechanical loads, the Hamilton principle has been used. The active vibration control for a single moving concentrated loading, thermal shock loading and a continuous stream of moving concentrated loadings has been investigated. Results, even if the thermal field is not full coupled, have shown that the control gain and velocity of moving loadings could have significant effects on the dynamic response and resonance of the system. The thermal field is not full coupled in [22], however in this work an analytical study for piezothermoelastic behavior of a functionally graded piezoelectric cylindrical shell subjected to axisymmetric thermal or mechanical loading has been proposed. Both direct and inverse piezoelectric effects have been considered and several numerical examples have been given and discussed to show the significant influence of material inhomogeneity. Kaminski and Corigliano [23] have shown the application of the generalized stochastic perturbation technique to thermo-piezoelectric analysis of solid continua, the discretization of the problem in terms of the stochastic perturbation-based Finite Element Method has also been provided. Montanaro [24] has demonstrated as the temperature on the outer bounding faces can be controlled in multilayered plates by the difference of electric potential between the faces. Abd-Alla and Mahmoud [25] have proposed a generalized magneto-thermoelastic model for orthotropic hollow cylinders when a thermal relaxation is generated. Further interesting papers about the thermo-electro-mechanical analysis have already been discussed in [3] for the cases of plate geometry.

The present work has three main aims:

- it gives a fully coupling between mechanical, thermal and electrical fields to analyze shells subjected to multifield loadings and to discuss the importance of multifield effects;
- it gives refined multifield two-dimensional models in order to overcome the main limitations of classical theories such those based on Kirchhoff [26] or Reissner/Mindlin [27, 28] hypotheses;
- shell geometries are investigated to show possible curvature effects.

The paper is organized in nine sections, after this introduction the constitutive equations for the thermo-electro-mechanical analysis have been obtained in Sect. 2 and the multifield geometrical relations for shell structures are discussed in Sect. 3. Section 4 has proposed the Carrera Unified Formulation (CUF) in order to obtain the shell refined two-dimensional models in both Equivalent Single Layer (ESL) and Layer Wise (LW) form, the Principle of Virtual Displacements (PVD) has been extended to thermo-electro-mechanical coupled problems in Sect. 5. Section 6 gives the Navier solution to obtain a closed form of the governing equations, Sect. 7 discusses the assembling procedure of fundamental nuclei and the acronyms for the refined models. The results have been discussed in Sect. 8 where some preliminary assessments and exhaustive thermo-electro-mechanical analyses of multilayered shells have been proposed. Section 9 gives the main conclusions.

2 Thermo-electro-mechanical constitutive equations

Constitutive equations characterize the individual material and its reaction to applied multifield loads, their thermo-electro-mechanical form is here obtained for

crystalline materials that shows piezoelectric properties, and piezoelectric polymers and semi-crystalline polymers with ferroelectric properties. Such materials must be polarized to express a piezoelectric effect, the external polarization is necessary to active the material. Depending on the chosen polarization, piezoelectric materials have a different coupling between the electric field and mechanical deformations or stresses. The materials considered in this work are polarized in z transverse normal direction. Thermodynamical principles and Maxwell relations [8, 9] are used to determine the general coupling between the mechanical, electrical and thermal fields. A *Gibbs free-energy function* G and a *thermopiezoelectric enthalpy density* H [4, 10] are defined as:

$$G(\epsilon_{ij}, \mathcal{E}_i, \theta) = \sigma_{ij}\epsilon_{ij} - \mathcal{E}_i\mathcal{D}_i - \eta\theta, \tag{1}$$

$$H(\epsilon_{ij}, \mathcal{E}_i, \theta, \vartheta_i) = G(\epsilon_{ij}, \mathcal{E}_i, \theta) - F(\vartheta_i), \tag{2}$$

σ_{ij} and ϵ_{ij} are the stress and strain components, $\mathcal{E}_i$ is the electric field vector, $\mathcal{D}_i$ is the electric displacement vector. η is the variation in entropy per unit of volume and θ is the over-temperature considered with respect to the reference temperature T_0. The function $F(\vartheta_i)$ depends on the spatial temperature gradient ϑ_i and it is defined as dissipation function:

$$F(\vartheta_i) = \frac{1}{2}\kappa_{ij}\vartheta_i\vartheta_j - \tau_0\dot{h}_i, \tag{3}$$

κ_{ij} is the symmetric, positive, semidefinite conductivity tensor, τ_0 is the thermal relaxation parameter and $\dot{h}_i$ is the temporal derivative of the heat flux h_i. The multifield problems analyzed in this work discard the relaxation parameter. Works [8, 9] and [10] give further details about the dissipation function $F(\vartheta_i)$.

The thermopiezoelectric enthalpy density H is written as a quadratic form in the case of a linear interaction:

$$\begin{aligned} H(\epsilon_{ij}, \mathcal{E}_i, \theta, \vartheta_i) &= \frac{1}{2}Q_{ijkl}\epsilon_{ij}\epsilon_{kl} - e_{ijk}\epsilon_{ij}\mathcal{E}_k - \lambda_{ij}\epsilon_{ij}\theta \\ &\quad - \frac{1}{2}\varepsilon_{kl}\mathcal{E}_k\mathcal{E}_l - p_k\mathcal{E}_k\theta - \frac{1}{2}\chi\theta^2 - \frac{1}{2}\kappa_{ij}\vartheta_i\vartheta_j, \end{aligned} \tag{4}$$

Q_{ijkl} is the elastic coefficients tensor considered for an orthotropic material in the problem reference system [2]. e_{ijk} are the piezoelectric coefficients and ε_{kl} are the permittivity coefficients [7]. λ_{ij} are the thermo-mechanical coupling coefficients, p_k are the pyroelectric coefficients, and $\chi = \frac{\rho C_v}{T_0}$ where ρ is the material density, C_v is the specific heat per unit mass and T_0 is the reference temperature [5].

The constitutive equations are obtained from the following partial derivatives:

$$\begin{aligned} \sigma_{ij} &= \frac{\partial H}{\partial \epsilon_{ij}}, \qquad \mathcal{D}_k = -\frac{\partial H}{\partial \mathcal{E}_k}, \\ \eta &= -\frac{\partial H}{\partial \theta}, \qquad h_i = -\frac{\partial H}{\partial \vartheta_i}. \end{aligned} \tag{5}$$

The constitutive equations for the thermo-electro-mechanical problem are obtained by substituting Eq. (4) in Eqs. (5):

$$\sigma_{ij} = Q_{ijkl}\epsilon_{kl} - e_{ijk}\mathcal{E}_k - \lambda_{ij}\theta, \tag{6}$$

$$\mathcal{D}_k = e_{ijk}\epsilon_{ij} + \varepsilon_{kl}\mathcal{E}_l + p_k\theta, \tag{7}$$

$$\eta = \lambda_{ij}\epsilon_{ij} + p_k\mathcal{E}_k + \chi\theta, \tag{8}$$

$$h_i = \kappa_{ij}\vartheta_j. \tag{9}$$

Equations (6)–(9) can be written in single-subscript notation by using the indexes $m = q = 1, 2, 3, 4, 5, 6$ and $i = j = 1, 2, 3$:

$$\sigma_m = Q_{mq}\epsilon_q - e_{mi}\mathcal{E}_i - \lambda_m\theta, \tag{10}$$

$$\mathcal{D}_i = e_{iq}\epsilon_q + \varepsilon_{ij}\mathcal{E}_j + p_i\theta, \tag{11}$$

$$\eta = \lambda_q\epsilon_q + p_j\mathcal{E}_j + \chi\theta, \tag{12}$$

$$h_i = \kappa_{ij}\vartheta_j. \tag{13}$$

Their matrix form can be obtained by indicating the matrices and vectors in bold scripture. Equations (10)–(13) are written for a generic k layer in the problem reference system (α, β, z) in the case of multilayered shells (see Fig. 1):

$$\boldsymbol{\sigma}^k = \boldsymbol{Q}^k\boldsymbol{\epsilon}^k - \boldsymbol{e}^{kT}\boldsymbol{\mathcal{E}}^k - \boldsymbol{\lambda}^k\theta^k, \tag{14}$$

$$\boldsymbol{\mathcal{D}}^k = \boldsymbol{e}^k\boldsymbol{\epsilon}^k + \boldsymbol{\varepsilon}^k\boldsymbol{\mathcal{E}}^k + \boldsymbol{p}^k\theta^k, \tag{15}$$

$$\eta^k = \boldsymbol{\lambda}^{kT}\boldsymbol{\epsilon}^k + \boldsymbol{p}^{kT}\boldsymbol{\mathcal{E}}^k + \chi^k\theta^k, \tag{16}$$

$$\boldsymbol{h}^k = \boldsymbol{\kappa}^k\boldsymbol{\vartheta}^k, \tag{17}$$

the over-temperature θ^k, the term χ^k and the entropy for unite volume η^k are scalar variables in each k layer.

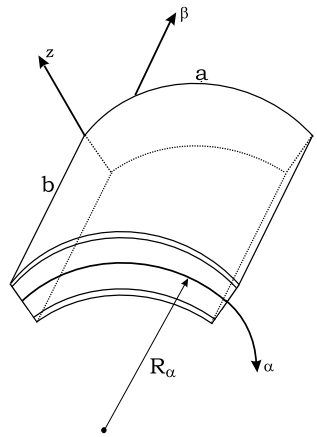

Fig. 1 Geometry and reference system for a multilayered smart shell

The 6×1 vectors of stress and strain components are:

$$\boldsymbol{\sigma}^k = \begin{Bmatrix} \sigma_{\alpha\alpha} \\ \sigma_{\beta\beta} \\ \sigma_{zz} \\ \sigma_{\beta z} \\ \sigma_{\alpha z} \\ \sigma_{\alpha\beta} \end{Bmatrix}^k, \qquad \boldsymbol{\epsilon}^k = \begin{Bmatrix} \epsilon_{\alpha\alpha} \\ \epsilon_{\beta\beta} \\ \epsilon_{zz} \\ \gamma_{\beta z} \\ \gamma_{\alpha z} \\ \gamma_{\alpha\beta} \end{Bmatrix}^k. \tag{18}$$

The 3×1 vectors of electrical displacement $\boldsymbol{\mathcal{D}}^k$, electrical field $\boldsymbol{\mathcal{E}}^k$, heat flux $\boldsymbol{h}^k$ and spatial gradient of temperature $\boldsymbol{\vartheta}^k$ are:

$$\begin{aligned} \boldsymbol{\mathcal{D}}^k &= \begin{Bmatrix} \mathcal{D}_\alpha \\ \mathcal{D}_\beta \\ \mathcal{D}_z \end{Bmatrix}^k, \qquad \boldsymbol{\mathcal{E}}^k = \begin{Bmatrix} \mathcal{E}_\alpha \\ \mathcal{E}_\beta \\ \mathcal{E}_z \end{Bmatrix}^k, \\ \boldsymbol{h}^k &= \begin{Bmatrix} h_\alpha \\ h_\beta \\ h_z \end{Bmatrix}^k, \qquad \boldsymbol{\vartheta}^k = \begin{Bmatrix} \vartheta_\alpha \\ \vartheta_\beta \\ \vartheta_z \end{Bmatrix}^k. \end{aligned} \tag{19}$$

The 3×1 array of pyroelectric coefficients $\boldsymbol{p}^k$ and the 6×1 array of thermo-mechanical coupling coefficients $\boldsymbol{\lambda}^k$ are:

$$\boldsymbol{p}^k = \begin{Bmatrix} p_1 \\ p_2 \\ p_3 \end{Bmatrix}^k, \qquad \boldsymbol{\lambda}^k = \boldsymbol{Q}^k \boldsymbol{\alpha}^k = \begin{Bmatrix} \lambda_1 \\ \lambda_2 \\ \lambda_3 \\ 0 \\ 0 \\ \lambda_6 \end{Bmatrix}^k, \tag{20}$$

where the elastic coefficients matrix $\boldsymbol{Q}^k$ of Hooke law in problem reference system for an orthotropic material is:

$$\boldsymbol{Q}^k = \begin{bmatrix} Q_{11} & Q_{12} & Q_{13} & 0 & 0 & Q_{16} \\ Q_{12} & Q_{22} & Q_{23} & 0 & 0 & Q_{26} \\ Q_{13} & Q_{23} & Q_{33} & 0 & 0 & Q_{36} \\ 0 & 0 & 0 & Q_{44} & Q_{45} & 0 \\ 0 & 0 & 0 & Q_{45} & Q_{55} & 0 \\ Q_{16} & Q_{26} & Q_{36} & 0 & 0 & Q_{66} \end{bmatrix}^k, \tag{21}$$

the vector $\boldsymbol{\alpha}^k$ has 6×1 dimension and it contains the thermal expansion coefficients:

$$\boldsymbol{\alpha}^k = \begin{Bmatrix} \alpha_1 \\ \alpha_2 \\ \alpha_3 \\ 0 \\ 0 \\ 0 \end{Bmatrix}^k. \tag{22}$$

The matrices $\boldsymbol{\varepsilon}^k$ of permittivity coefficients and $\boldsymbol{\kappa}^k$ of conductivity coefficients have 3×3 dimension:

$$\begin{aligned} \boldsymbol{\varepsilon}^k &= \begin{bmatrix} \varepsilon_{11} & \varepsilon_{12} & 0 \\ \varepsilon_{12} & \varepsilon_{22} & 0 \\ 0 & 0 & \varepsilon_{33} \end{bmatrix}^k, \\ \boldsymbol{\kappa}^k &= \begin{bmatrix} \kappa_{11} & \kappa_{12} & 0 \\ \kappa_{12} & \kappa_{22} & 0 \\ 0 & 0 & \kappa_{33} \end{bmatrix}^k. \end{aligned} \tag{23}$$

The matrix of piezoelectric coefficients $\boldsymbol{e}^k$ has 3×6 dimension:

$$\boldsymbol{e}^k = \begin{bmatrix} 0 & 0 & 0 & e_{14} & e_{15} & 0 \\ 0 & 0 & 0 & e_{24} & e_{25} & 0 \\ e_{31} & e_{32} & e_{33} & 0 & 0 & e_{36} \end{bmatrix}^k. \tag{24}$$

The Principle of Virtual Displacements, which will be extended to thermo-electro-mechanical problems in Sect. 5, uses Eqs. (14)–(17) opportunely split in in-plane components (subscript p) and out-of-plane components (subscript n). Other two new subscripts are introduced: the subscript C for those variables in the variational statement which need the substitution of constitutive equations; the subscript G for those variables in constitutive equations which need the substitution of shell geometrical relations (see the next section). The split stress and strain component vectors

are:

$$\boldsymbol{\sigma}_{pC}^{k}=\left\{\begin{array}{c}\sigma_{\alpha\alpha}\\ \sigma_{\beta\beta}\\ \sigma_{\alpha\beta}\end{array}\right\}^{k},\qquad \boldsymbol{\sigma}_{nC}^{k}=\left\{\begin{array}{c}\sigma_{\alpha z}\\ \sigma_{\beta z}\\ \sigma_{zz}\end{array}\right\}^{k},$$
$$\boldsymbol{\epsilon}_{pG}^{k}=\left\{\begin{array}{c}\epsilon_{\alpha\alpha}\\ \epsilon_{\beta\beta}\\ \gamma_{\alpha\beta}\end{array}\right\}^{k},\qquad \boldsymbol{\epsilon}_{nG}^{k}=\left\{\begin{array}{c}\gamma_{\alpha z}\\ \gamma_{\beta z}\\ \epsilon_{zz}\end{array}\right\}^{k}. \tag{25}$$

The 3×1 vectors of electrical displacement, electrical field, heat flux and spatial gradient of the temperature, split in in-plane and out-of-plane components, are:

$$\begin{aligned}\boldsymbol{\mathcal{D}}_{pC}^{k}&=\left\{\begin{array}{c}\mathcal{D}_{\alpha}\\ \mathcal{D}_{\beta}\end{array}\right\}^{k},\qquad \boldsymbol{\mathcal{D}}_{nC}^{k}=\left\{\mathcal{D}_{z}\right\}^{k},\\ \boldsymbol{\mathcal{E}}_{pG}^{k}&=\left\{\begin{array}{c}\mathcal{E}_{\alpha}\\ \mathcal{E}_{\beta}\end{array}\right\}^{k},\qquad \boldsymbol{\mathcal{E}}_{nG}^{k}=\left\{\mathcal{E}_{z}\right\}^{k},\\ \boldsymbol{h}_{pC}^{k}&=\left\{\begin{array}{c}h_{\alpha}\\ h_{\beta}\end{array}\right\}^{k},\qquad \boldsymbol{h}_{nC}^{k}=\left\{h_{z}\right\}^{k},\\ \boldsymbol{\vartheta}_{pG}^{k}&=\left\{\begin{array}{c}\vartheta_{\alpha}\\ \vartheta_{\beta}\end{array}\right\}^{k},\qquad \boldsymbol{\vartheta}_{nG}^{k}=\left\{\vartheta_{z}\right\}^{k}.\end{aligned} \tag{26}$$

The split form of Eqs. (14)–(17) is obtained by considering Eqs. (25) and (26):

$$\begin{aligned}\boldsymbol{\sigma}_{pC}^{k}&=\boldsymbol{Q}_{pp}^{k}\boldsymbol{\epsilon}_{pG}^{k}+\boldsymbol{Q}_{pn}^{k}\boldsymbol{\epsilon}_{nG}^{k}-\boldsymbol{e}_{pp}^{kT}\boldsymbol{\mathcal{E}}_{pG}^{k}\\ &\quad-\boldsymbol{e}_{np}^{kT}\boldsymbol{\mathcal{E}}_{nG}^{k}-\boldsymbol{\lambda}_{p}^{k}\theta^{k},\end{aligned} \tag{27}$$

$$\begin{aligned}\boldsymbol{\sigma}_{nC}^{k}&=\boldsymbol{Q}_{np}^{k}\boldsymbol{\epsilon}_{pG}^{k}+\boldsymbol{Q}_{nn}^{k}\boldsymbol{\epsilon}_{nG}^{k}-\boldsymbol{e}_{pn}^{kT}\boldsymbol{\mathcal{E}}_{pG}^{k}\\ &\quad-\boldsymbol{e}_{nn}^{kT}\boldsymbol{\mathcal{E}}_{nG}^{k}-\boldsymbol{\lambda}_{n}^{k}\theta^{k},\end{aligned} \tag{28}$$

$$\begin{aligned}\boldsymbol{\mathcal{D}}_{pC}^{k}&=\boldsymbol{e}_{pp}^{k}\boldsymbol{\epsilon}_{pG}^{k}+\boldsymbol{e}_{pn}^{k}\boldsymbol{\epsilon}_{nG}^{k}+\boldsymbol{\varepsilon}_{pp}^{k}\boldsymbol{\mathcal{E}}_{pG}^{k}\\ &\quad+\boldsymbol{\varepsilon}_{pn}^{k}\boldsymbol{\mathcal{E}}_{nG}^{k}+\boldsymbol{p}_{p}^{k}\theta^{k},\end{aligned} \tag{29}$$

$$\begin{aligned}\boldsymbol{\mathcal{D}}_{nC}^{k}&=\boldsymbol{e}_{np}^{k}\boldsymbol{\epsilon}_{pG}^{k}+\boldsymbol{e}_{nn}^{k}\boldsymbol{\epsilon}_{nG}^{k}+\boldsymbol{\varepsilon}_{np}^{k}\boldsymbol{\mathcal{E}}_{pG}^{k}\\ &\quad+\boldsymbol{\varepsilon}_{nn}^{k}\boldsymbol{\mathcal{E}}_{nG}^{k}+\boldsymbol{p}_{n}^{k}\theta^{k},\end{aligned} \tag{30}$$

$$\begin{aligned}\eta_{C}^{k}&=\boldsymbol{\lambda}_{p}^{kT}\boldsymbol{\epsilon}_{pG}^{k}+\boldsymbol{\lambda}_{n}^{kT}\boldsymbol{\epsilon}_{nG}^{k}+\boldsymbol{p}_{p}^{kT}\boldsymbol{\mathcal{E}}_{pG}^{k}\\ &\quad+\boldsymbol{p}_{n}^{kT}\boldsymbol{\mathcal{E}}_{nG}^{k}+\chi^{k}\theta^{k},\end{aligned} \tag{31}$$

$$\boldsymbol{h}_{p}^{k}=\boldsymbol{\kappa}_{pp}^{k}\boldsymbol{\vartheta}_{pG}^{k}+\boldsymbol{\kappa}_{pn}^{k}\boldsymbol{\vartheta}_{nG}^{k}, \tag{32}$$

$$\boldsymbol{h}_{n}^{k}=\boldsymbol{\kappa}_{np}^{k}\boldsymbol{\vartheta}_{pG}^{k}+\boldsymbol{\kappa}_{nn}^{k}\boldsymbol{\vartheta}_{nG}^{k}. \tag{33}$$

The explicit forms of the new matrices in Eqs. (27)–(33) are:

- Elastic coefficients:

$$\begin{aligned}\boldsymbol{Q}_{pp}^{k}&=\begin{bmatrix}Q_{11}&Q_{12}&Q_{16}\\ Q_{12}&Q_{22}&Q_{26}\\ Q_{16}&Q_{26}&Q_{66}\end{bmatrix}^{k},\\ \boldsymbol{Q}_{pn}^{k}&=\begin{bmatrix}0&0&Q_{13}\\ 0&0&Q_{23}\\ 0&0&Q_{36}\end{bmatrix}^{k},\\ \boldsymbol{Q}_{np}^{k}&=\begin{bmatrix}0&0&0\\ 0&0&0\\ Q_{13}&Q_{23}&Q_{36}\end{bmatrix}^{k},\\ \boldsymbol{Q}_{nn}^{k}&=\begin{bmatrix}Q_{55}&Q_{45}&0\\ Q_{45}&Q_{44}&0\\ 0&0&Q_{33}\end{bmatrix}^{k}.\end{aligned} \tag{34}$$

- Piezoelectric coefficients:

$$\begin{aligned}&\boldsymbol{e}_{pp}^{k}=\begin{bmatrix}0&0&0\\ 0&0&0\end{bmatrix}^{k},\qquad \boldsymbol{e}_{pn}^{k}=\begin{bmatrix}e_{15}&e_{14}&0\\ e_{25}&e_{24}&0\end{bmatrix}^{k},\\ &\boldsymbol{e}_{np}^{k}=\begin{bmatrix}e_{31}&e_{32}&e_{36}\end{bmatrix}^{k},\qquad \boldsymbol{e}_{nn}^{k}=\begin{bmatrix}0&0&e_{33}\end{bmatrix}^{k}.\end{aligned} \tag{35}$$

- Permittivity coefficients:

$$\begin{aligned}&\boldsymbol{\varepsilon}_{pp}^{k}=\begin{bmatrix}\varepsilon_{11}&\varepsilon_{12}\\ \varepsilon_{12}&\varepsilon_{22}\end{bmatrix}^{k},\qquad \boldsymbol{\varepsilon}_{pn}^{k}=\begin{bmatrix}0\\ 0\end{bmatrix}^{k},\\ &\boldsymbol{\varepsilon}_{np}^{k}=\begin{bmatrix}0&0\end{bmatrix}^{k},\qquad \boldsymbol{\varepsilon}_{nn}^{k}=\begin{bmatrix}\varepsilon_{33}\end{bmatrix}^{k}.\end{aligned} \tag{36}$$

- Thermo-mechanical coupling coefficients:

$$\boldsymbol{\lambda}_{p}^{k}=\begin{bmatrix}\lambda_{1}\\ \lambda_{2}\\ \lambda_{6}\end{bmatrix}^{k},\qquad \boldsymbol{\lambda}_{n}^{k}=\begin{bmatrix}0\\ 0\\ \lambda_{3}\end{bmatrix}^{k}. \tag{37}$$

- Pyroelectric coefficients:

$$\boldsymbol{p}_{p}^{k}=\begin{bmatrix}p_{1}\\ p_{2}\end{bmatrix}^{k},\qquad \boldsymbol{p}_{n}^{k}=\begin{bmatrix}p_{3}\end{bmatrix}^{k}. \tag{38}$$

- Conductivity coefficients:

$$\begin{aligned}&\boldsymbol{\kappa}_{pp}^{k}=\begin{bmatrix}\kappa_{11}&\kappa_{12}\\ \kappa_{12}&\kappa_{22}\end{bmatrix}^{k},\qquad \boldsymbol{\kappa}_{pn}^{k}=\begin{bmatrix}0\\ 0\end{bmatrix}^{k},\\ &\boldsymbol{\kappa}_{np}^{k}=\begin{bmatrix}0&0\end{bmatrix}^{k},\qquad \boldsymbol{\kappa}_{nn}^{k}=\begin{bmatrix}\kappa_{33}\end{bmatrix}^{k}.\end{aligned} \tag{39}$$

3 Geometrical relations for shells

A thin shell is defined as a two-dimensional structure because it is a three-dimensional body bounded by two

closely spaced curved surfaces where one dimension (the distance between the two surfaces) is small in comparison with the other two dimensions in the plane directions. The middle surface of the shell is the locus of points which lie midway between these surfaces. The distance between the surfaces measured along the normal to the middle surface is the *thickness* of the shell at that point [29]. Geometry and the reference system are indicated in Fig. 1. The square of an infinitesimal linear segment in the layer, the associated infinitesimal area and volume are defined as:

$$ds_k^2 = H_\alpha^{k\,2}\, d\alpha_k^2 + H_\beta^{k\,2}\, d\beta_k^2 + H_z^{k\,2}\, dz_k^2, \tag{40}$$

$$d\Omega_k = H_\alpha^k H_\beta^k\, d\alpha_k\, d\beta_k, \tag{41}$$

$$dV_k = H_\alpha^k H_\beta^k H_z^k\, d\alpha_k\, d\beta_k\, dz_k, \tag{42}$$

where the metric coefficients are:

$$\begin{aligned} H_\alpha^k &= A^k\big(1 + z_k/R_\alpha^k\big), \\ H_\beta^k &= B^k\big(1 + z_k/R_\beta^k\big), \qquad H_z^k = 1. \end{aligned} \tag{43}$$

k indicates the kth-layer of the multilayered shell; R_α^k and R_β^k are the principal radii of curvature along the coordinates α_k and β_k, respectively. A^k and B^k are the coefficients of the first fundamental form of Ω_k (Γ_k is the Ω_k boundary). In this work, we will focus only to shells with constant radii of curvature (cylindrical, spherical, toroidal geometries) for which $A^k = B^k = 1$. Further details about shell structures can be found in [29] and [30]. The thermo-electro-mechanical geometrical relations for shells link the strains with the displacement vector, the electric field components with the electric potential and the spatial gradient of temperature with the scalar over-temperature. They are split in in-plane (p) and out-of-plane (n) components:

$$\boldsymbol{\epsilon}_{pG}^k = [\epsilon_{\alpha\alpha}, \epsilon_{\beta\beta}, \gamma_{\alpha\beta}]^{kT} = \big(\boldsymbol{D}_p^k + \boldsymbol{A}_p^k\big)\boldsymbol{u}^k, \tag{44}$$

$$\boldsymbol{\epsilon}_{nG}^k = [\gamma_{\alpha z}, \gamma_{\beta z}, \epsilon_{zz}]^{kT} = \big(\boldsymbol{D}_{np}^k + \boldsymbol{D}_{nz}^k - \boldsymbol{A}_n^k\big)\boldsymbol{u}^k, \tag{45}$$

$$\boldsymbol{\mathcal{E}}_{pG}^k = [\mathcal{E}_\alpha, \mathcal{E}_\beta]^{kT} = -\boldsymbol{D}_{ep}^k \Phi^k, \tag{46}$$

$$\boldsymbol{\mathcal{E}}_{nG}^k = [\mathcal{E}_z]^k = -\boldsymbol{D}_{en}^k\, \Phi^k, \tag{47}$$

$$\boldsymbol{\vartheta}_{pG}^k = [\vartheta_\alpha, \vartheta_\beta]^{kT} = -\boldsymbol{D}_{tp}^k \theta^k, \tag{48}$$

$$\boldsymbol{\vartheta}_{nG}^k = [\vartheta_z]^k = -\boldsymbol{D}_{tn}^k \theta^k, \tag{49}$$

$\boldsymbol{\epsilon}_{pG}^k$ and $\boldsymbol{\epsilon}_{nG}^k$ are the in-plane and transverse strains, respectively. $\boldsymbol{u}^k = (u, v, w)^k$ is the displacement vector. $\boldsymbol{\mathcal{E}}_{nG}^k$ and $\boldsymbol{\mathcal{E}}_{pG}^k$ are in-plane and transverse electric field components, respectively. Φ^k is the scalar electric potential. $\boldsymbol{\vartheta}_{pG}^k$ and $\boldsymbol{\vartheta}_{nG}^k$ are in-plane and transverse spatial gradients of temperature, respectively. θ^k is the scalar over-temperature referred to the reference external room temperature. T means the transpose of a vector. The explicit form of the introduced arrays follows:

$$\begin{aligned} \boldsymbol{D}_p^k &= \begin{bmatrix} \frac{\partial_{\alpha_k}}{H_\alpha^k} & 0 & 0 \\ 0 & \frac{\partial_{\beta_k}}{H_\beta^k} & 0 \\ \frac{\partial_{\beta_k}}{H_\beta^k} & \frac{\partial_{\alpha_k}}{H_\alpha^k} & 0 \end{bmatrix}, \qquad \boldsymbol{D}_{np}^k = \begin{bmatrix} 0 & 0 & \frac{\partial_{\alpha_k}}{H_\alpha^k} \\ 0 & 0 & \frac{\partial_{\beta_k}}{H_\beta^k} \\ 0 & 0 & 0 \end{bmatrix}, \\ \boldsymbol{D}_{nz}^k &= \begin{bmatrix} \partial_{z_k} & 0 & 0 \\ 0 & \partial_{z_k} & 0 \\ 0 & 0 & \partial_{z_k} \end{bmatrix}, \qquad \boldsymbol{D}_{ep}^k = \begin{bmatrix} \frac{\partial_{\alpha_k}}{H_\alpha^k} \\ \\ \frac{\partial_{\beta_k}}{H_\beta^k} \end{bmatrix}, \\ \boldsymbol{D}_{en}^k &= \begin{bmatrix} \partial_{z_k} \end{bmatrix}, \end{aligned} \tag{50}$$

$$\begin{aligned} \boldsymbol{D}_{tp}^k &= \begin{bmatrix} \frac{\partial_{\alpha_k}}{H_\alpha^k} \\ \\ \frac{\partial_{\beta_k}}{H_\beta^k} \end{bmatrix}, \qquad \boldsymbol{D}_{tn}^k = \begin{bmatrix} \partial_{z_k} \end{bmatrix}, \\ \boldsymbol{A}_p^k &= \begin{bmatrix} 0 & 0 & \frac{1}{H_\alpha^k R_\alpha^k} \\ 0 & 0 & \frac{1}{H_\beta^k R_\beta^k} \\ 0 & 0 & 0 \end{bmatrix}, \\ \boldsymbol{A}_n^k &= \begin{bmatrix} \frac{1}{H_\alpha^k R_\alpha^k} & 0 & 0 \\ 0 & \frac{1}{H_\beta^k R_\beta^k} & 0 \\ 0 & 0 & 0 \end{bmatrix}. \end{aligned} \tag{51}$$

The symbols in differential operators matrices indicate the partial derivatives $\partial_{\alpha_k} = \frac{\partial}{\partial \alpha_k}$, $\partial_{\beta_k} = \frac{\partial}{\partial \beta_k}$ and $\partial_{z_k} = \frac{\partial}{\partial z_k}$. The parameters H_α^k and H_β^k equal 1 for plate geometries, in these cases the radii of curvature R_α^k and R_β^k are infinite and the pure geometrical contributes $\boldsymbol{A}_p^k$ and $\boldsymbol{A}_n^k$ become zero.

4 Carrera Unified Formulation (CUF) for refined 2D models

A large variety of refined two-dimensional models for multifield analysis of multilayered structures are here

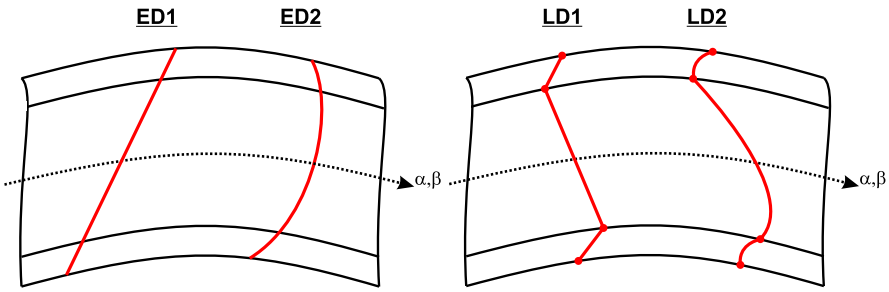

Fig. 2 Equivalent Single Layer (ESL) vs. Layer Wise (LW) theories for the thermo-electro-mechanical variables of a multilayered smart shell

obtained by means of the Carrera Unified Formulation (CUF) [1, 2]. The governing equations are written, in a unified manner, in terms of a few fundamental nuclei which do not formally depend on the order of expansion N used in the thickness direction and on the description of variables at the multilayer level. The multilayer description can be equivalent single layer (ESL) (when the variable is assumed for the whole multilayered structure) or layer wise (LW) (when the variable is independently considered in each layer). A two-dimensional shell theory allows the unknown variables to be expressed as a set of thickness functions that only depend on the thickness coordinate z and the correspondent variable which depends on the curved coordinates α and β. A generic variable $\boldsymbol{f}(\alpha, \beta, z)$ (displacements, electric potential or over-temperature) and its variation $\delta \boldsymbol{f}(\alpha, \beta, z)$ are written according to the following general expansion:

$$\begin{aligned} &\boldsymbol{f}(\alpha, \beta, z) = F_\tau(z)\boldsymbol{f}_\tau(\alpha, \beta), \\ &\delta\boldsymbol{f}(\alpha, \beta, z) = F_s(z)\delta\boldsymbol{f}_s(\alpha, \beta), \\ &\quad \text{with } \tau, s = 1, \ldots, N, \end{aligned} \tag{52}$$

the bold letters denote arrays, (α, β) are the in-plane curved coordinates and z the thickness one. The summing convention, with repeated indexes τ and s, is assumed. The order of expansion N goes from first to fourth order. In the thermo-electro-mechanical shell models, displacements can be modelled in both ESL or LW form, over-temperature and electric potential are always considered in LW form. Therefore, a two-dimensional thermo-electro-mechanical shell model is defined as ESL or LW, depending on the choice made for the displacement vector.

4.1 Equivalent Single Layer (ESL) approach

The displacement $\boldsymbol{u} = (u, v, w)$ is modelled in equivalent single layer (ESL) form when the unknowns are the same for the whole multilayered shell [2] (see the left part of Fig. 2 where a first and second order of expansion in a three-layered shell are proposed). The z description is obtained via a Taylor expansion:

$$\begin{aligned} u &= F_0 u_0 + F_1 u_1 + \cdots + F_N u_N = F_\tau u_\tau, \\ v &= F_0 v_0 + F_1 v_1 + \cdots + F_N v_N = F_\tau v_\tau, \\ w &= F_0 w_0 + F_1 w_1 + \cdots + F_N w_N = F_\tau w_\tau, \end{aligned} \tag{53}$$

with $\tau = 0, 1, \ldots, N$; N is the order of expansion that ranges from 1 (linear) to 4:

$$F_0 = z^0 = 1, \qquad F_1 = z^1 = z, \quad \ldots, \quad F_N = z^N. \tag{54}$$

The vectorial form of Eq. (53) is:

$$\begin{aligned} &\boldsymbol{u}(\alpha, \beta, z) = F_\tau(z)\boldsymbol{u}_\tau(\alpha, \beta), \\ &\delta\boldsymbol{u}(\alpha, \beta, z) = F_s(z)\delta\boldsymbol{u}_s(\alpha, \beta), \\ &\quad \text{with } \tau, s = 1, \ldots, N. \end{aligned} \tag{55}$$

Simpler theories, such those which discard the ϵ_{zz} effect, can be obtained from refined ESL models. First order Shear Deformation Theory (FSDT) [27, 28] comes from an ESL model with linear expansion in the thickness direction z where a constant transverse displacement w in z is imposed. Classical Lamination Theory (CLT) [26] is obtained from FSDT by imposing an infinite transverse shear rigidity.

4.2 Layer Wise (LW) approach

A layer wise (LW) approach is possible when each layer of a multilayered shell is described as an inde-

pendent structure [2]. The displacement $\boldsymbol{u}^k = (u, v, w)^k$ is modelled for each k layer in order to automatically obtain the zigzag form of displacement in multilayered transverse anisotropic shells, see for example the right part of Fig. 2 where a first and second order of expansion through the thickness direction of a three-layered shell are given. The z expansion for displacement components is made for each k layer:

$$\begin{aligned} u^k &= F_0 u_0^k + F_1 u_1^k + \cdots + F_N u_N^k = F_\tau u_\tau^k, \\ v^k &= F_0 v_0^k + F_1 v_1^k + \cdots + F_N v_N^k = F_\tau v_\tau^k, \\ w^k &= F_0 w_0^k + F_1 w_1^k + \cdots + F_N w_N^k = F_\tau w_\tau^k, \end{aligned} \tag{56}$$

with $\tau = 0, 1, \ldots, N$, N is the order of expansion that ranges from 1 (linear) to 4. $k = 1, \ldots, N_l$, where N_l indicates the number of layers. Equation (56) can also be given in a vectorial form:

$$\begin{aligned} &\boldsymbol{u}^k(\alpha, \beta, z) = F_\tau(z) \boldsymbol{u}_\tau^k(\alpha, \beta), \\ &\delta\boldsymbol{u}^k(\alpha, \beta, z) = F_s(z) \delta\boldsymbol{u}_s^k(\alpha, \beta), \\ &\quad \text{with } \tau, s = t, b, r \quad \text{and} \quad k = 1, \ldots, N_l, \end{aligned} \tag{57}$$

where t and b indicate the top and bottom of each k layer, respectively; r indicates the higher orders of expansion in the thickness direction: $r = 2, \ldots, N$. The thickness functions $F_\tau(\zeta_k)$ and $F_s(\zeta_k)$ are defined at the kth-layer level and they are a linear combination of Legendre polynomials $P_j = P_j(\zeta_k)$ of the jth-order defined in ζ_k-domain ($\zeta_k = \frac{2z_k}{h_k}$ with z_k local coordinate and h_k thickness, both referred to kth layer, so $-1 \le \zeta_k \le 1$). The first five Legendre polynomials are:

$$\begin{aligned} &P_0 = 1, \qquad P_1 = \zeta_k, \qquad P_2 = \frac{(3{\zeta_k}^2 - 1)}{2}, \\ &P_3 = \frac{5{\zeta_k}^3}{2} - \frac{3\zeta_k}{2}, \qquad P_4 = \frac{35{\zeta_k}^4}{8} - \frac{15{\zeta_k}^2}{4} + \frac{3}{8}, \end{aligned} \tag{58}$$

and they are combined in the thickness functions as:

$$\begin{aligned} &F_t = F_0 = \frac{P_0 + P_1}{2}, \qquad F_b = F_1 = \frac{P_0 - P_1}{2}, \\ &F_r = P_r - P_{r-2} \quad \text{with } r = 2, \ldots, N. \end{aligned} \tag{59}$$

They have the following interesting properties:

$$\zeta_k = 1: \quad F_t = 1; \quad F_b = 0; \quad F_r = 0 \quad \text{at top}, \tag{60}$$

$$\zeta_k = -1: \quad F_t = 0; \quad F_b = 1; \quad F_r = 0 \text{ at bottom}, \tag{61}$$

which means that interface values of the variables are considered as variable unknowns, see Fig. 2. This feature permits to easily impose the compatibility conditions for displacements at each layer interface.

In case of thermo-electro-mechanical problems, the primary variables are the displacement vector $\boldsymbol{u} = (u, v, w)$, the scalar electric potential Φ and the scalar over-temperature θ ($\theta = T_1 - T_0$ where temperature T_1 is referred to the reference external room temperature T_0). The variables Φ^k and θ^k are always modelled as LW because of their higher spatial gradient:

$$\begin{aligned} &\Phi^k(\alpha, \beta, z) = F_\tau(z) \Phi_\tau^k(\alpha, \beta), \\ &\delta\Phi^k(\alpha, \beta, z) = F_s(z) \delta\Phi_s^k(\alpha, \beta), \\ &\quad \text{with } \tau, s = t, b, r \quad \text{and} \quad k = 1, \ldots, N_l, \end{aligned} \tag{62}$$

$$\begin{aligned} &\theta^k(\alpha, \beta, z) = F_\tau(z) \theta_\tau^k(\alpha, \beta), \\ &\delta\theta^k(\alpha, \beta, z) = F_s(z) \delta\theta_s^k(\alpha, \beta), \\ &\quad \text{with } \tau, s = t, b, r \quad \text{and} \quad k = 1, \ldots, N_l, \end{aligned} \tag{63}$$

the meanings of the subscripts and superscripts are the same already discussed for the LW form of the displacements.

5 Multifield Principle of Virtual Displacements (PVD)

The virtual internal electrical and thermal works are introduced into the Principle of Virtual Displacements (PVD) in case of fully coupling between the mechanical, electrical and thermal fields. This variational statement is:

$$\begin{aligned} &\int_V \big(\delta\boldsymbol{\epsilon}_{pG}^T \boldsymbol{\sigma}_{pC} + \delta\boldsymbol{\epsilon}_{nG}^T \boldsymbol{\sigma}_{nC} - \delta\boldsymbol{\mathcal{E}}_{pG}^T \boldsymbol{\mathcal{D}}_{pC} - \delta\boldsymbol{\mathcal{E}}_{nG}^T \boldsymbol{\mathcal{D}}_{nC} \\ &\qquad - \delta\theta\eta_C - \delta\boldsymbol{\vartheta}_{pG}^T \boldsymbol{h}_{pC} - \delta\boldsymbol{\vartheta}_{nG}^T \boldsymbol{h}_{nC}\big)\, dV \\ &\quad = \delta L_e - \delta L_{in}. \end{aligned} \tag{64}$$

The total volume V is considered as a summation on the number of layers N_l where the volume V_k for each k layer is an integral on the in-plane surface Ω_k plus an integral in the thickness direction domain A_k:

$$\begin{aligned} &\sum_{k=1}^{N_l} \int_{\Omega_k} \int_{A_k} \big\{\delta\boldsymbol{\epsilon}_{pG}^{kT} \boldsymbol{\sigma}_{pC}^k + \delta\boldsymbol{\epsilon}_{nG}^{kT} \boldsymbol{\sigma}_{nC}^k - \delta\boldsymbol{\mathcal{E}}_{pG}^{kT} \boldsymbol{\mathcal{D}}_{pC}^k \\ &\qquad - \delta\boldsymbol{\mathcal{E}}_{nG}^{kT} \boldsymbol{\mathcal{D}}_{nC}^k - \delta\theta^k \eta_C^k - \delta\boldsymbol{\vartheta}_{pG}^{kT} \boldsymbol{h}_{pC}^k \end{aligned}$$

$$
\begin{aligned}
&- \delta \boldsymbol{\vartheta}_{nG}^{kT} \boldsymbol{h}_{nC}^{k} \big\} \, d\Omega_k \, dz \\
&= \sum_{k=1}^{N_l} \delta L_e^k - \sum_{k=1}^{N_l} \delta L_{in}^k,
\end{aligned} \tag{65}
$$

δL_e^k and δL_{in}^k are the external and inertial virtual work at the k-layer level, respectively.

The governing equations have the following form:

$$
\begin{aligned}
\delta \boldsymbol{u}_s^k: \quad & \boldsymbol{K}_{uu}^{k\tau s} \boldsymbol{u}_\tau^k + \boldsymbol{K}_{u\Phi}^{k\tau s} \Phi_\tau^k + \boldsymbol{K}_{u\theta}^{k\tau s} \theta_\tau^k \\
& = \boldsymbol{p}_{us}^k - \boldsymbol{M}_{uu}^{k\tau s} \ddot{\boldsymbol{u}}_\tau^k, \\
\delta \Phi_s^k: \quad & \boldsymbol{K}_{\Phi u}^{k\tau s} \boldsymbol{u}_\tau^k + \boldsymbol{K}_{\Phi\Phi}^{k\tau s} \Phi_\tau^k + \boldsymbol{K}_{\Phi\theta}^{k\tau s} \theta_\tau^k = \boldsymbol{p}_{\Phi s}^k, \\
\delta \theta_s^k: \quad & \boldsymbol{K}_{\theta u}^{k\tau s} \boldsymbol{u}_\tau^k + \boldsymbol{K}_{\theta\Phi}^{k\tau s} \Phi_\tau^k + \boldsymbol{K}_{\theta\theta}^{k\tau s} \theta_\tau^k = \boldsymbol{p}_{\theta s}^k.
\end{aligned} \tag{66}
$$

The arrays $\boldsymbol{p}_{us}^k$, $\boldsymbol{p}_{\Phi s}^k$ and $\boldsymbol{p}_{\theta s}^k$ indicate the variationally consistent mechanical, electrical and thermal loadings, respectively. Along with these governing equations the following boundary conditions on the edge Γ_k of the in-plane integration domain Ω_k hold:

$$
\begin{aligned}
&\boldsymbol{\Pi}_{uu}^{k\tau s} \boldsymbol{u}_\tau^k + \boldsymbol{\Pi}_{u\Phi}^{k\tau s} \Phi_\tau^k + \boldsymbol{\Pi}_{u\theta}^{k\tau s} \theta_\tau^k \\
&\quad = \boldsymbol{\Pi}_{uu}^{k\tau s} \bar{\boldsymbol{u}}_\tau^k + \boldsymbol{\Pi}_{u\Phi}^{k\tau s} \bar{\Phi}_\tau^k + \boldsymbol{\Pi}_{u\theta}^{k\tau s} \bar{\theta}_\tau^k, \\
&\boldsymbol{\Pi}_{\Phi u}^{k\tau s} \boldsymbol{u}_\tau^k + \boldsymbol{\Pi}_{\Phi\Phi}^{k\tau s} \Phi_\tau^k + \boldsymbol{\Pi}_{\Phi\theta}^{k\tau s} \theta_\tau^k \\
&\quad = \boldsymbol{\Pi}_{\Phi u}^{k\tau s} \bar{\boldsymbol{u}}_\tau^k + \boldsymbol{\Pi}_{\Phi\Phi}^{k\tau s} \bar{\Phi}_\tau^k + \boldsymbol{\Pi}_{\Phi\theta}^{k\tau s} \bar{\theta}_\tau^k, \\
&\boldsymbol{\Pi}_{\theta u}^{k\tau s} \boldsymbol{u}_\tau^k + \boldsymbol{\Pi}_{\theta\Phi}^{k\tau s} \Phi_\tau^k + \boldsymbol{\Pi}_{\theta\theta}^{k\tau s} \theta_\tau^k \\
&\quad = \boldsymbol{\Pi}_{\theta u}^{k\tau s} \bar{\boldsymbol{u}}_\tau^k + \boldsymbol{\Pi}_{\theta\Phi}^{k\tau s} \bar{\Phi}_\tau^k + \boldsymbol{\Pi}_{\theta\theta}^{k\tau s} \bar{\theta}_\tau^k.
\end{aligned} \tag{67}
$$

The electric potential Φ^k and the over-temperature θ^k are variables of the problem in addition to the displacement $\boldsymbol{u}^k$ which can be seen in ESL or LW form. Independently by the choice made for the displacements, the electric potential and the over-temperature are always seen in LW form.

In this work the variational statement includes only the internal thermal work made by the temperature in the case of mechanical load or imposed electric potential applied on the structure; it includes only the internal thermal work made by the gradient of temperature in the case of temperature applied at the top and bottom of the structure.

5.1 PVD: mechanical load and imposed electric potential

In case of mechanical load or electric potential applied on the structure, in Eq. (65) the terms $\delta \boldsymbol{\vartheta}_{pG}^{k\,T} \boldsymbol{h}_{pC}^k$ and $\delta \boldsymbol{\vartheta}_{nG}^{k\,T} \boldsymbol{h}_{nC}^k$ are not considered because it does not exist a gradient of temperature. The variational statement is:

$$
\begin{aligned}
&\sum_{k=1}^{N_l} \int_{\Omega_k} \int_{A_k} \big\{ \delta \boldsymbol{\epsilon}_{pG}^{kT} \boldsymbol{\sigma}_{pC}^k + \delta \boldsymbol{\epsilon}_{nG}^{kT} \boldsymbol{\sigma}_{nC}^k - \delta \boldsymbol{\mathcal{E}}_{pG}^{kT} \boldsymbol{\mathcal{D}}_{pC}^k \\
&\quad - \delta \boldsymbol{\mathcal{E}}_{nG}^{kT} \boldsymbol{\mathcal{D}}_{nC}^k - \delta \theta^k \eta_C^k \big\} \, d\Omega_k \, dz \\
&= \sum_{k=1}^{N_l} \delta L_e^k - \sum_{k=1}^{N_l} \delta L_{in}^k.
\end{aligned} \tag{68}
$$

We can simply discard the heat fluxes $\boldsymbol{h}_{pC}^k$ and $\boldsymbol{h}_{nC}^k$ in the constitutive equations as obtained in Eqs. (27)–(33):

$$
\begin{aligned}
\boldsymbol{\sigma}_{pC}^k &= \boldsymbol{Q}_{pp}^k \boldsymbol{\epsilon}_{pG}^k + \boldsymbol{Q}_{pn}^k \boldsymbol{\epsilon}_{nG}^k - \boldsymbol{e}_{pp}^{kT} \boldsymbol{\mathcal{E}}_{pG}^k \\
&\quad - \boldsymbol{e}_{np}^{kT} \boldsymbol{\mathcal{E}}_{nG}^k - \boldsymbol{\lambda}_p^k \theta^k,
\end{aligned} \tag{69}
$$

$$
\begin{aligned}
\boldsymbol{\sigma}_{nC}^k &= \boldsymbol{Q}_{np}^k \boldsymbol{\epsilon}_{pG}^k + \boldsymbol{Q}_{nn}^k \boldsymbol{\epsilon}_{nG}^k - \boldsymbol{e}_{pn}^{kT} \boldsymbol{\mathcal{E}}_{pG}^k \\
&\quad - \boldsymbol{e}_{nn}^{kT} \boldsymbol{\mathcal{E}}_{nG}^k - \boldsymbol{\lambda}_n^k \theta^k,
\end{aligned} \tag{70}
$$

$$
\begin{aligned}
\boldsymbol{\mathcal{D}}_{pC}^k &= \boldsymbol{e}_{pp}^k \boldsymbol{\epsilon}_{pG}^k + \boldsymbol{e}_{pn}^k \boldsymbol{\epsilon}_{nG}^k + \boldsymbol{\varepsilon}_{pp}^k \boldsymbol{\mathcal{E}}_{pG}^k \\
&\quad + \boldsymbol{\varepsilon}_{pn}^k \boldsymbol{\mathcal{E}}_{nG}^k + \boldsymbol{p}_p^k \theta^k,
\end{aligned} \tag{71}
$$

$$
\begin{aligned}
\boldsymbol{\mathcal{D}}_{nC}^k &= \boldsymbol{e}_{np}^k \boldsymbol{\epsilon}_{pG}^k + \boldsymbol{e}_{nn}^k \boldsymbol{\epsilon}_{nG}^k + \boldsymbol{\varepsilon}_{np}^k \boldsymbol{\mathcal{E}}_{pG}^k \\
&\quad + \boldsymbol{\varepsilon}_{nn}^k \boldsymbol{\mathcal{E}}_{nG}^k + \boldsymbol{p}_n^k \theta^k,
\end{aligned} \tag{72}
$$

$$
\begin{aligned}
\eta_C^k &= \boldsymbol{\lambda}_p^{kT} \boldsymbol{\epsilon}_{pG}^k + \boldsymbol{\lambda}_n^{kT} \boldsymbol{\epsilon}_{nG}^k + \boldsymbol{p}_p^{kT} \boldsymbol{\mathcal{E}}_{pG}^k \\
&\quad + \boldsymbol{p}_n^{kT} \boldsymbol{\mathcal{E}}_{nG}^k + \chi^k \theta^k.
\end{aligned} \tag{73}
$$

The geometrical relations for shells have been described in Sect. 3 and CUF for the refined two-dimensional models has been detailed in Sect. 4. Equation (68) is rewritten for a generic k layer as:

$$
\begin{aligned}
&\int_{\Omega_k} \int_{A_k} \big[\big(\big(\boldsymbol{D}_p^k + \boldsymbol{A}_p^k \big) F_s \delta \boldsymbol{u}_s^k \big)^T \big(\big(\boldsymbol{Q}_{pp}^k \big(\boldsymbol{D}_p^k + \boldsymbol{A}_p^k \big) + \boldsymbol{Q}_{pn}^k \big(\boldsymbol{D}_{np}^k + \boldsymbol{D}_{nz}^k - \boldsymbol{A}_n^k \big) \big) F_\tau \boldsymbol{u}_\tau^k + \boldsymbol{e}_{pp}^{kT} \boldsymbol{D}_{ep}^k F_\tau \Phi_\tau^k \\
&\quad + \boldsymbol{e}_{np}^{kT} \boldsymbol{D}_{en}^k F_\tau \Phi_\tau^k - \boldsymbol{\lambda}_p^k F_\tau \theta_\tau^k \big) + \big(\big(\boldsymbol{D}_{np}^k + \boldsymbol{D}_{nz}^k - \boldsymbol{A}_n^k \big) F_s \delta \boldsymbol{u}_s^k \big)^T \big(\big(\boldsymbol{Q}_{np}^k \big(\boldsymbol{D}_p^k + \boldsymbol{A}_p^k \big) + \boldsymbol{Q}_{nn}^k \big(\boldsymbol{D}_{np}^k + \boldsymbol{D}_{nz}^k - \boldsymbol{A}_n^k \big) \big)
\end{aligned}
$$

$$\times F_\tau \boldsymbol{u}_\tau^k + \boldsymbol{e}_{pn}^{kT} \boldsymbol{D}_{ep}^k F_\tau \Phi_\tau^k + \boldsymbol{e}_{nn}^{kT} \boldsymbol{D}_{en}^k F_\tau \Phi_\tau^k - \boldsymbol{\lambda}_n^k F_\tau \theta_\tau^k) + (\boldsymbol{D}_{ep}^k F_s \delta \Phi_s^k)^T \big((\boldsymbol{e}_{pp}^k (\boldsymbol{D}_p^k + \boldsymbol{A}_p^k) + \boldsymbol{e}_{pn}^k (\boldsymbol{D}_{np}^k + \boldsymbol{D}_{nz}^k - \boldsymbol{A}_n^k)) F_\tau \boldsymbol{u}_\tau^k - \boldsymbol{\varepsilon}_{pp}^k \boldsymbol{D}_{ep}^k F_\tau \Phi_\tau^k - \boldsymbol{\varepsilon}_{pn}^k \boldsymbol{D}_{en}^k F_\tau \Phi_\tau^k + \boldsymbol{p}_p^k F_\tau \theta_\tau^k) + (\boldsymbol{D}_{en}^k F_s \delta \Phi_s^k)^T \big((\boldsymbol{e}_{np}^k (\boldsymbol{D}_p^k + \boldsymbol{A}_p^k) + \boldsymbol{e}_{nn}^k (\boldsymbol{D}_{np}^k + \boldsymbol{D}_{nz}^k - \boldsymbol{A}_n^k)) F_\tau \boldsymbol{u}_\tau^k - \boldsymbol{\varepsilon}_{np}^k \boldsymbol{D}_{ep}^k F_\tau \Phi_\tau^k - \boldsymbol{\varepsilon}_{nn}^k \boldsymbol{D}_{en}^k F_\tau \Phi_\tau^k + \boldsymbol{p}_n^k F_\tau \theta_\tau^k) - F_s \delta \theta_s^{kT} \big((\boldsymbol{\lambda}_p^{kT} (\boldsymbol{D}_p^k + \boldsymbol{A}_p^k) + \boldsymbol{\lambda}_n^{kT} (\boldsymbol{D}_{np}^k + \boldsymbol{D}_{nz}^k - \boldsymbol{A}_n^k)) F_\tau \boldsymbol{u}_\tau^k - \boldsymbol{p}_p^{kT} \boldsymbol{D}_{ep}^k F_\tau \Phi_\tau^k - \boldsymbol{p}_n^{kT} \boldsymbol{D}_{en}^k F_\tau \Phi_\tau^k + \chi^k F_\tau \theta_\tau^k) \big] d\Omega_k \, dz$$

$$= \delta L_e^k - \delta L_{in}^k. \tag{74}$$

Integrating by parts Eq. (74) (as suggested in [6] and [7]), the fundamental nuclei are obtained after the comparison with the governing relations in Eqs. (66):

$$\boldsymbol{K}_{uu}^{k\tau s} = \int_{A_k} \big[(-\boldsymbol{D}_p^k + \boldsymbol{A}_p^k)^T \big(\boldsymbol{Q}_{pp}^k (\boldsymbol{D}_p^k + \boldsymbol{A}_p^k) + \boldsymbol{Q}_{pn}^k (\boldsymbol{D}_{np}^k + \boldsymbol{D}_{nz}^k - \boldsymbol{A}_n^k) \big) + (-\boldsymbol{D}_{np}^k + \boldsymbol{D}_{nz}^k - \boldsymbol{A}_n^k)^T \times \big(\boldsymbol{Q}_{np}^k (\boldsymbol{D}_p^k + \boldsymbol{A}_p^k) + \boldsymbol{Q}_{nn}^k (\boldsymbol{D}_{np}^k + \boldsymbol{D}_{nz}^k - \boldsymbol{A}_n^k) \big) \big] F_s F_\tau H_\alpha^k H_\beta^k \, dz, \tag{75}$$

$$\boldsymbol{K}_{u\Phi}^{k\tau s} = \int_{A_k} \big[(-\boldsymbol{D}_p^k + \boldsymbol{A}_p^k)^T \big(\boldsymbol{e}_{pp}^{kT} \boldsymbol{D}_{ep}^k + \boldsymbol{e}_{np}^{kT} \boldsymbol{D}_{en}^k \big) + (-\boldsymbol{D}_{np}^k + \boldsymbol{D}_{nz}^k - \boldsymbol{A}_n^k)^T \big(\boldsymbol{e}_{pn}^{kT} \boldsymbol{D}_{ep}^k + \boldsymbol{e}_{nn}^{kT} \boldsymbol{D}_{en}^k \big) \big] F_s F_\tau H_\alpha^k H_\beta^k \, dz, \tag{76}$$

$$\boldsymbol{K}_{u\theta}^{k\tau s} = \int_{A_k} \big[(-\boldsymbol{D}_p^k + \boldsymbol{A}_p^k)^T (-\boldsymbol{\lambda}_p^k) + (-\boldsymbol{D}_{np}^k + \boldsymbol{D}_{nz}^k - \boldsymbol{A}_n^k)^T (-\boldsymbol{\lambda}_n^k) \big] F_s F_\tau H_\alpha^k H_\beta^k \, dz, \tag{77}$$

$$\boldsymbol{K}_{\Phi u}^{k\tau s} = \int_{A_k} \big[(-\boldsymbol{D}_{ep}^k)^T \big(\boldsymbol{e}_{pp}^k (\boldsymbol{D}_p^k + \boldsymbol{A}_p^k) + \boldsymbol{e}_{pn}^k (\boldsymbol{D}_{np}^k + \boldsymbol{D}_{nz}^k - \boldsymbol{A}_n^k) \big) + (\boldsymbol{D}_{en}^k)^T \big(\boldsymbol{e}_{np}^k (\boldsymbol{D}_p^k + \boldsymbol{A}_p^k) + \boldsymbol{e}_{nn}^k (\boldsymbol{D}_{np}^k + \boldsymbol{D}_{nz}^k - \boldsymbol{A}_n^k) \big) \big] F_s F_\tau H_\alpha^k H_\beta^k \, dz, \tag{78}$$

$$\boldsymbol{K}_{\Phi\Phi}^{k\tau s} = \int_{A_k} \big[(\boldsymbol{D}_{ep}^k)^T \big(\boldsymbol{\varepsilon}_{pp}^k \boldsymbol{D}_{ep}^k + \boldsymbol{\varepsilon}_{pn}^k \boldsymbol{D}_{en}^k \big) - (\boldsymbol{D}_{en}^k)^T \big(\boldsymbol{\varepsilon}_{np}^k \boldsymbol{D}_{ep}^k + \boldsymbol{\varepsilon}_{nn}^k \boldsymbol{D}_{en}^k \big) \big] F_s F_\tau H_\alpha^k H_\beta^k \, dz, \tag{79}$$

$$\boldsymbol{K}_{\Phi\theta}^{k\tau s} = \int_{A_k} \big[-\boldsymbol{D}_{ep}^{kT} \boldsymbol{p}_p^k + \boldsymbol{D}_{en}^{kT} \boldsymbol{p}_n^k \big] F_s F_\tau H_\alpha^k H_\beta^k \, dz, \tag{80}$$

$$\boldsymbol{K}_{\theta u}^{k\tau s} = \int_{A_k} \big[-\boldsymbol{\lambda}_p^{kT} (\boldsymbol{D}_p^k + \boldsymbol{A}_p^k) - \boldsymbol{\lambda}_n^{kT} (\boldsymbol{D}_{np}^k + \boldsymbol{D}_{nz}^k - \boldsymbol{A}_n^k) \big] F_s F_\tau H_\alpha^k H_\beta^k \, dz, \tag{81}$$

$$\boldsymbol{K}_{\theta\Phi}^{k\tau s} = \int_{A_k} \big[\boldsymbol{p}_p^{kT} \boldsymbol{D}_{ep}^k + \boldsymbol{p}_n^{kT} \boldsymbol{D}_{en}^k \big] F_s F_\tau H_\alpha^k H_\beta^k \, dz, \tag{82}$$

$$\boldsymbol{K}_{\theta\theta}^{k\tau s} = \int_{A_k} -\chi^k F_s F_\tau H_\alpha^k H_\beta^k \, dz. \tag{83}$$

The nuclei for boundary conditions on the edge Γ_k are obtained from the comparison with Eqs. (67):

$$\boldsymbol{\Pi}_{uu}^{k\tau s} = \int_{A_k} \big[\boldsymbol{I}_p^{kT} \big(\boldsymbol{Q}_{pp}^k (\boldsymbol{D}_p^k + \boldsymbol{A}_p^k) + \boldsymbol{Q}_{pn}^k (\boldsymbol{D}_{np}^k + \boldsymbol{D}_{nz}^k - \boldsymbol{A}_n^k) \big) + \boldsymbol{I}_{np}^{kT} \big(\boldsymbol{Q}_{np}^k (\boldsymbol{D}_p^k + \boldsymbol{A}_p^k) + \boldsymbol{Q}_{nn}^k (\boldsymbol{D}_{np}^k + \boldsymbol{D}_{nz}^k - \boldsymbol{A}_n^k) \big) \big] F_s F_\tau H_\alpha^k H_\beta^k \, dz, \tag{84}$$

$$\boldsymbol{\Pi}_{u\Phi}^{k\tau s} = \int_{A_k} \big[\boldsymbol{I}_p^{kT} \big(\boldsymbol{e}_{pp}^{kT} \boldsymbol{D}_{ep}^k + \boldsymbol{e}_{np}^{kT} \boldsymbol{D}_{en}^k \big) + \boldsymbol{I}_{np}^{kT} \big(\boldsymbol{e}_{pn}^{kT} \boldsymbol{D}_{ep}^k + \boldsymbol{e}_{nn}^{kT} \boldsymbol{D}_{en}^k \big) \big] F_s F_\tau H_\alpha^k H_\beta^k \, dz, \tag{85}$$

$$\boldsymbol{\Pi}_{u\theta}^{k\tau s} = \int_{A_k} \big[-\boldsymbol{I}_p^{kT} \boldsymbol{\lambda}_p^k - \boldsymbol{I}_{np}^{kT} \boldsymbol{\lambda}_n^k \big] F_s F_\tau H_\alpha^k H_\beta^k \, dz, \tag{86}$$

$$\boldsymbol{\Pi}^{k\tau s}_{\Phi u} = \int_{A_k} \big[\boldsymbol{I}^{kT}_{ep}\big(\boldsymbol{e}^k_{pp}\big(\boldsymbol{D}^k_p + \boldsymbol{A}^k_p\big) + \boldsymbol{e}^k_{pn}\big(\boldsymbol{D}^k_{np} + \boldsymbol{D}^k_{nz} - \boldsymbol{A}^k_n\big)\big)\big] F_s F_\tau H^k_\alpha H^k_\beta \, dz, \tag{87}$$

$$\boldsymbol{\Pi}^{k\tau s}_{\Phi\Phi} = \int_{A_k} \big[-\boldsymbol{I}^{kT}_{ep}\big(\boldsymbol{\varepsilon}^k_{pp}\boldsymbol{D}^k_{ep} + \boldsymbol{\varepsilon}^k_{pn}\boldsymbol{D}^k_{en}\big)\big] \times F_s F_\tau H^k_\alpha H^k_\beta \, dz, \tag{88}$$

$$\boldsymbol{\Pi}^{k\tau s}_{\Phi\theta} = \int_{A_k} \big[\boldsymbol{I}^{kT}_{ep}\boldsymbol{p}^k_p\big] F_s F_\tau H^k_\alpha H^k_\beta \, dz, \tag{89}$$

$$\boldsymbol{\Pi}^{k\tau s}_{\theta u} = 0, \tag{90}$$

$$\boldsymbol{\Pi}^{k\tau s}_{\theta\Phi} = 0, \tag{91}$$

$$\boldsymbol{\Pi}^{k\tau s}_{\theta\theta} = 0. \tag{92}$$

$\boldsymbol{I}^k_p$ and $\boldsymbol{I}^k_{np}$ are (3×3) matrices, to perform the integration by parts, obtained from $\boldsymbol{D}^k_p$ and $\boldsymbol{D}^k_{np}$ simply replacing the differential operators with 1. $\boldsymbol{I}^k_{ep}$ has (2×1) dimension, it permits to perform the integration by parts and it is obtained from the matrix $\boldsymbol{D}^k_{ep}$ simply replacing the differential operators with 1. Nuclei, given in Eqs. (75)–(83), are used in the governing equation (66) in the case of mechanical load or electric potential applied on the shell surfaces. In this case, in Eqs. (66) the inertial contribute and the thermal load are discarded. The electric potential is directly imposed in the vector Φ^k_τ; therefore, the electric load $\boldsymbol{p}^k_{\Phi s}$ is not considered. Nuclei for boundary conditions in Eqs. (84)–(92) are used in the boundary conditions of Eqs. (67) in the case of applied mechanical load or imposed electric potential.

5.2 PVD: imposed temperature

In case of temperature imposed on the external surfaces of the structure, the term $\delta\theta^k \eta^k_C$ is not considered in Eq. (65) in order to allow the "classical" thermal stress analysis of smart shells. Therefore, the variational statement is:

$$\sum_{k=1}^{N_l} \int_{\Omega_k} \int_{A_k} \big\{\delta\boldsymbol{\epsilon}^{k\,T}_{pG}\boldsymbol{\sigma}^k_{pC} + \delta\boldsymbol{\epsilon}^{k\,T}_{nG}\boldsymbol{\sigma}^k_{nC} - \delta\boldsymbol{\mathcal{E}}^{k\,T}_{pG}\boldsymbol{\mathcal{D}}^k_{pC} - \delta\boldsymbol{\mathcal{E}}^{k\,T}_{nG}\boldsymbol{\mathcal{D}}^k_{nC} - \delta\boldsymbol{\vartheta}^T_{pG}\boldsymbol{h}_{pC} - \delta\boldsymbol{\vartheta}^T_{nG}\boldsymbol{h}_{nC}\big\} \, d\Omega_k \, dz = \sum_{k=1}^{N_l} \delta L^k_e - \sum_{k=1}^{N_l} \delta L^k_{in}. \tag{93}$$

The entropy η^k_c is discarded in the constitutive equations obtained in Eqs. (27)–(33):

$$\boldsymbol{\sigma}^k_{pC} = \boldsymbol{Q}^k_{pp}\boldsymbol{\epsilon}^k_{pG} + \boldsymbol{Q}^k_{pn}\boldsymbol{\epsilon}^k_{nG} - \boldsymbol{e}^{kT}_{pp}\boldsymbol{\mathcal{E}}^k_{pG} - \boldsymbol{e}^{kT}_{np}\boldsymbol{\mathcal{E}}^k_{nG} - \boldsymbol{\lambda}^k_p\theta^k, \tag{94}$$

$$\boldsymbol{\sigma}^k_{nC} = \boldsymbol{Q}^k_{np}\boldsymbol{\epsilon}^k_{pG} + \boldsymbol{Q}^k_{nn}\boldsymbol{\epsilon}^k_{nG} - \boldsymbol{e}^{kT}_{pn}\boldsymbol{\mathcal{E}}^k_{pG} - \boldsymbol{e}^{kT}_{nn}\boldsymbol{\mathcal{E}}^k_{nG} - \boldsymbol{\lambda}^k_n\theta^k, \tag{95}$$

$$\boldsymbol{\mathcal{D}}^k_{pC} = \boldsymbol{e}^k_{pp}\boldsymbol{\epsilon}^k_{pG} + \boldsymbol{e}^k_{pn}\boldsymbol{\epsilon}^k_{nG} + \boldsymbol{\varepsilon}^k_{pp}\boldsymbol{\mathcal{E}}^k_{pG} + \boldsymbol{\varepsilon}^k_{pn}\boldsymbol{\mathcal{E}}^k_{nG} + \boldsymbol{p}^k_p\theta^k, \tag{96}$$

$$\boldsymbol{\mathcal{D}}^k_{nC} = \boldsymbol{e}^k_{np}\boldsymbol{\epsilon}^k_{pG} + \boldsymbol{e}^k_{nn}\boldsymbol{\epsilon}^k_{nG} + \boldsymbol{\varepsilon}^k_{np}\boldsymbol{\mathcal{E}}^k_{pG} + \boldsymbol{\varepsilon}^k_{nn}\boldsymbol{\mathcal{E}}^k_{nG} + \boldsymbol{p}^k_n\theta^k, \tag{97}$$

$$\boldsymbol{h}^k_p = \boldsymbol{\kappa}^k_{pp}\boldsymbol{\vartheta}^k_{pG} + \boldsymbol{\kappa}^k_{pn}\boldsymbol{\vartheta}^k_{nG}, \tag{98}$$

$$\boldsymbol{h}^k_n = \boldsymbol{\kappa}^k_{np}\boldsymbol{\vartheta}^k_{pG} + \boldsymbol{\kappa}^k_{nn}\boldsymbol{\vartheta}^k_{nG}. \tag{99}$$

The geometrical relations for shells are those of Sect. 3 and the Carrera Unified Formulation has been described in Sect. 4. Equation (93) is rewritten in the following form for a generic k layer:

$$\int_{\Omega_k}\int_{A_k} \big[\big(\big(\boldsymbol{D}^k_p + \boldsymbol{A}^k_p\big)F_s\delta\boldsymbol{u}^k_s\big)^T\big(\big(\boldsymbol{Q}^k_{pp}\big(\boldsymbol{D}^k_p + \boldsymbol{A}^k_p\big) + \boldsymbol{Q}^k_{pn}\big(\boldsymbol{D}^k_{np} + \boldsymbol{D}^k_{nz} - \boldsymbol{A}^k_n\big)\big)F_\tau\boldsymbol{u}^k_\tau + \boldsymbol{e}^{kT}_{pp}\boldsymbol{D}^k_{ep}F_\tau\Phi^k_\tau + \boldsymbol{e}^{kT}_{np}\boldsymbol{D}^k_{en}F_\tau\Phi^k_\tau - \boldsymbol{\lambda}^k_pF_\tau\theta^k_\tau\big) + \big(\big(\boldsymbol{D}^k_{np} + \boldsymbol{D}^k_{nz} - \boldsymbol{A}^k_n\big)F_s\delta\boldsymbol{u}^k_s\big)^T\big(\big(\boldsymbol{Q}^k_{np}\big(\boldsymbol{D}^k_p + \boldsymbol{A}^k_p\big) + \boldsymbol{Q}^k_{nn}\big(\boldsymbol{D}^k_{np} + \boldsymbol{D}^k_{nz} - \boldsymbol{A}^k_n\big)\big) \times F_\tau\boldsymbol{u}^k_\tau + \boldsymbol{e}^{kT}_{pn}\boldsymbol{D}^k_{ep}F_\tau\Phi^k_\tau + \boldsymbol{e}^{kT}_{nn}\boldsymbol{D}^k_{en}F_\tau\Phi^k_\tau - \boldsymbol{\lambda}^k_nF_\tau\theta^k_\tau\big) + \big(\boldsymbol{D}^k_{ep}F_s\delta\Phi^k_s\big)^T\big(\big(\boldsymbol{e}^k_{pp}\big(\boldsymbol{D}^k_p + \boldsymbol{A}^k_p\big) + \boldsymbol{e}^k_{pn}\big(\boldsymbol{D}^k_{np} + \boldsymbol{D}^k_{nz} - \boldsymbol{A}^k_n\big)\big)F_\tau\boldsymbol{u}^k_\tau - \boldsymbol{\varepsilon}^k_{pp}\boldsymbol{D}^k_{ep}F_\tau\Phi^k_\tau - \boldsymbol{\varepsilon}^k_{pn}\boldsymbol{D}^k_{en}F_\tau\Phi^k_\tau + \boldsymbol{p}^k_pF_\tau\theta^k_\tau\big) + \big(\boldsymbol{D}^k_{en}F_s\delta\Phi^k_s\big)^T\big(\big(\boldsymbol{e}^k_{np}\big(\boldsymbol{D}^k_p + \boldsymbol{A}^k_p\big) + \boldsymbol{e}^k_{nn}\big(\boldsymbol{D}^k_{np} + \boldsymbol{D}^k_{nz} - \boldsymbol{A}^k_n\big)\big)F_\tau\boldsymbol{u}^k_\tau - \boldsymbol{\varepsilon}^k_{np}\boldsymbol{D}^k_{ep}F_\tau\Phi^k_\tau - \boldsymbol{\varepsilon}^k_{nn}\boldsymbol{D}^k_{en}F_\tau\Phi^k_\tau + \boldsymbol{p}^k_nF_\tau\theta^k_\tau\big) + \big(\boldsymbol{D}^k_{tp}F_s\delta\theta^k_s\big)^T$$

$$\times \left(\boldsymbol{\kappa}_{pp}^{k}\left(-\boldsymbol{D}_{tp}^{k}\right)F_{\tau}\theta_{\tau}^{k}+\boldsymbol{\kappa}_{pn}^{k}\left(-\boldsymbol{D}_{tn}^{k}\right)F_{\tau}\theta_{\tau}^{k}\right)+\left(\boldsymbol{D}_{tn}^{k}F_{s}\delta\theta_{s}^{k}\right)^{T}\left(\boldsymbol{\kappa}_{np}^{k}\left(-\boldsymbol{D}_{tp}^{k}\right)F_{\tau}\theta_{\tau}^{k}+\boldsymbol{\kappa}_{nn}^{k}\left(-\boldsymbol{D}_{tn}^{k}\right)F_{\tau}\theta_{\tau}^{k}\right)\Big]d\Omega_{k}\,dz$$
$$=\delta L_{e}^{k}-\delta L_{in}^{k}. \tag{100}$$

Integrating by parts Eq. (100), as suggested in [6] and [7], the fundamental nuclei $\boldsymbol{K}_{uu}^{k\tau s}$, $\boldsymbol{K}_{u\Phi}^{k\tau s}$, $\boldsymbol{K}_{u\theta}^{k\tau s}$, $\boldsymbol{K}_{\Phi u}^{k\tau s}$, $\boldsymbol{K}_{\Phi\Phi}^{k\tau s}$ and $\boldsymbol{K}_{\Phi\theta}^{k\tau s}$ are the same of PVD in Sect. 5.1 for the applied mechanical load or imposed electric potential, while nuclei $\boldsymbol{K}_{\theta u}^{k\tau s}$, $\boldsymbol{K}_{\theta\Phi}^{k\tau s}$ and $\boldsymbol{K}_{\theta\theta}^{k\tau s}$ are:

$$\boldsymbol{K}_{\theta u}^{k\tau s}=0, \tag{101}$$

$$\boldsymbol{K}_{\theta\Phi}^{k\tau s}=0, \tag{102}$$

$$\boldsymbol{K}_{\theta\theta}^{k\tau s}=\int_{A_k}\Big[\left(\boldsymbol{D}_{tp}^{k}\right)^{T}\left(\boldsymbol{\kappa}_{pp}^{k}\boldsymbol{D}_{tp}^{k}+\boldsymbol{\kappa}_{pn}^{k}\boldsymbol{D}_{tn}^{k}\right)-\left(\boldsymbol{D}_{tn}^{k}\right)^{T}\times\left(\boldsymbol{\kappa}_{np}^{k}\boldsymbol{D}_{tp}^{k}+\boldsymbol{\kappa}_{nn}^{k}\boldsymbol{D}_{tn}^{k}\right)\Big]F_{s}F_{\tau}H_{\alpha}^{k}H_{\beta}^{k}\,dz. \tag{103}$$

Nuclei for boundary conditions on the edge Γ_k $\boldsymbol{\Pi}_{uu}^{k\tau s}$, $\boldsymbol{\Pi}_{u\Phi}^{k\tau s}$, $\boldsymbol{\Pi}_{u\theta}^{k\tau s}$, $\boldsymbol{\Pi}_{\Phi u}^{k\tau s}$, $\boldsymbol{\Pi}_{\Phi\Phi}^{k\tau s}$, $\boldsymbol{\Pi}_{\Phi\theta}^{k\tau s}$, $\boldsymbol{\Pi}_{\theta u}^{k\tau s}$ and $\boldsymbol{\Pi}_{\theta\Phi}^{k\tau s}$ are the same of PVD in Sect. 5.1 for the applied mechanical load or imposed electric potential, while nucleus $\boldsymbol{\Pi}_{\theta\theta}^{k\tau s}$ is different:

$$\boldsymbol{\Pi}_{\theta\theta}^{k\tau s}=\int_{A_k}\Big[\left(-\boldsymbol{I}_{tp}^{k}\right)^{T}\left(\boldsymbol{\kappa}_{pp}^{k}\boldsymbol{D}_{tp}^{k}+\boldsymbol{\kappa}_{pn}^{k}\boldsymbol{D}_{tn}^{k}\right)\Big]\times F_{s}F_{\tau}H_{\alpha}^{k}H_{\beta}^{k}\,dz, \tag{104}$$

$\boldsymbol{I}_{tp}^{k}$ has (2×1) dimension and it permits to perform the integration by parts, it comes from the matrix $\boldsymbol{D}_{tp}^{k}$ simply replacing the differential operators with 1. Nuclei, here obtained, are used in the governing equations (66) in the case of imposed temperature on the surfaces. In this case, in Eqs. (66) the mechanical and electrical loads and the inertial contribute are discarded. The temperature is directly imposed in the vector θ_{τ}^{k}; therefore, the thermal load $\boldsymbol{p}_{\theta s}^{k}$ is not considered. Nuclei for boundary conditions here discussed are introduced in the boundary conditions of Eqs. (67) in the case of imposed temperature on the surfaces.

6 Navier solution

The following integrals in the z-thickness direction are defined in order to write the explicit form of fundamental nuclei obtained in Sects. 5.1 and 5.2:

$$\begin{aligned}
&\left(J^{k\tau s},J_{\alpha}^{k\tau s},J_{\beta}^{k\tau s},J_{\frac{\alpha}{\beta}}^{k\tau s},J_{\frac{\beta}{\alpha}}^{k\tau s},J_{\alpha\beta}^{k\tau s}\right)\\
&\quad=\int_{A_k}F_{\tau}F_{s}\left(1,H_{\alpha}^{k},H_{\beta}^{k},\frac{H_{\alpha}^{k}}{H_{\beta}^{k}},\frac{H_{\beta}^{k}}{H_{\alpha}^{k}},H_{\alpha}^{k}H_{\beta}^{k}\right)dz,\\
&\left(J^{k\tau_{z}s},J_{\alpha}^{k\tau_{z}s},J_{\beta}^{k\tau_{z}s},J_{\frac{\alpha}{\beta}}^{k\tau_{z}s},J_{\frac{\beta}{\alpha}}^{k\tau_{z}s},J_{\alpha\beta}^{k\tau_{z}s}\right)\\
&\quad=\int_{A_k}\frac{\partial F_{\tau}}{\partial z}F_{s}\left(1,H_{\alpha}^{k},H_{\beta}^{k},\frac{H_{\alpha}^{k}}{H_{\beta}^{k}},\frac{H_{\beta}^{k}}{H_{\alpha}^{k}},H_{\alpha}^{k}H_{\beta}^{k}\right)dz,\\
&\left(J^{k\tau s_{z}},J_{\alpha}^{k\tau s_{z}},J_{\beta}^{k\tau s_{z}},J_{\frac{\alpha}{\beta}}^{k\tau s_{z}},J_{\frac{\beta}{\alpha}}^{k\tau s_{z}},J_{\alpha\beta}^{k\tau s_{z}}\right)\\
&\quad=\int_{A_k}F_{\tau}\frac{\partial F_{s}}{\partial z}\left(1,H_{\alpha}^{k},H_{\beta}^{k},\frac{H_{\alpha}^{k}}{H_{\beta}^{k}},\frac{H_{\beta}^{k}}{H_{\alpha}^{k}},H_{\alpha}^{k}H_{\beta}^{k}\right)dz,\\
&\left(J^{k\tau_{z}s_{z}},J_{\alpha}^{k\tau_{z}s_{z}},J_{\beta}^{k\tau_{z}s_{z}},J_{\frac{\alpha}{\beta}}^{k\tau_{z}s_{z}},J_{\frac{\beta}{\alpha}}^{k\tau_{z}s_{z}},J_{\alpha\beta}^{k\tau_{z}s_{z}}\right)\\
&\quad=\int_{A_k}\frac{\partial F_{\tau}}{\partial z}\frac{\partial F_{s}}{\partial z}\left(1,H_{\alpha}^{k},H_{\beta}^{k},\frac{H_{\alpha}^{k}}{H_{\beta}^{k}},\frac{H_{\beta}^{k}}{H_{\alpha}^{k}},H_{\alpha}^{k}H_{\beta}^{k}\right)dz.
\end{aligned} \tag{105}$$

The explicit forms of fundamental nuclei are obtained by developing the matrices products and using the z-integrals in Eqs. (105).

Navier-type closed form solution is possible if harmonic expressions for the displacements, electric potential and over-temperature are considered and if the following material coefficients are zero: $Q_{16}=Q_{26}=Q_{36}=Q_{45}=0$, $\varepsilon_{12}=p_{1}=p_{2}=e_{25}=e_{14}=e_{36}=0$ and $\lambda_{6}=\kappa_{12}=0$. The harmonic assumptions for the primary variables correspond to simply supported boundary conditions:

$$\begin{aligned}
u_{\tau}^{k}&=\sum_{m,n}\left(\hat{U}_{\tau}^{k}\right)\cos\left(\frac{m\pi\alpha}{a}\right)\sin\left(\frac{n\pi\beta}{b}\right),\\
&\quad k=1,N_{l},\\
v_{\tau}^{k}&=\sum_{m,n}\left(\hat{V}_{\tau}^{k}\right)\sin\left(\frac{m\pi\alpha}{a}\right)\cos\left(\frac{n\pi\beta}{b}\right),\\
&\quad \tau=t,b,r,\\
&\left(w_{\tau}^{k},\Phi_{\tau}^{k},\theta_{\tau}^{k}\right)\\
&\quad=\sum_{m,n}\left(\hat{W}_{\tau}^{k},\hat{\Phi}_{\tau}^{k},\hat{\theta}_{\tau}^{k}\right)\sin\left(\frac{m\pi\alpha}{a}\right)\sin\left(\frac{n\pi\beta}{b}\right),\\
&\quad r=2,N,
\end{aligned} \tag{106}$$

$\hat{U}_{\tau}^{k}$, $\hat{V}_{\tau}^{k}$, $\hat{W}_{\tau}^{k}$, $\hat{\Phi}_{\tau}^{k}$, $\hat{\theta}_{\tau}^{k}$ are the amplitudes.

The explicit closed form of fundamental nuclei is given in the Appendix.

7 Assembling procedure and acronyms employed

The fundamental nuclei explicitly given in Sect. 6 and Appendix can be expanded for the chosen order N and assembled at the multilayer level. By expanding via indexes τ, s, the order of expansion N from 1 to 4 in the thickness direction is considered. The expanded matrices are obtained for each layer, and then the index k allows the multilayer assembling procedure, which can either be ESL or LW.

A system of acronyms must be given to define the refined two-dimensional models developed in this work for the thermo-electro-mechanical analysis of multilayered shells. Displacements can be in ESL or LW form, while the electric potential and the over-temperature are always considered in LW form. Therefore, a two-dimensional model is defined as ESL or LW depending on the choice made for the displacement. ESL models are indicated as ED1–ED4, where E means the ESL approach, D means that the Principle of Virtual Displacements or their extensions to thermo-electro-mechanical analysis have been employed; the last digit, from 1 to 4, indicates the order of expansion in the thickness direction for displacements, electric potential and over-temperature. The letter E is replaced by the letter L in the case of LW approaches, the relative models are indicated as LD1–LD4. In the case of a multifield analysis, additional parentheses are introduced in the acronyms: (u, Φ, θ) means fully coupled thermo-electro-mechanical models, (u, Φ) is added in the case of fully coupled electro-mechanical analysis, (u, θ) is added in the case of fully coupled thermo-mechanical analysis and (u) means pure mechanical problem. The models including only two or one physical fields are simply obtained by deleting the opportune rows and columns in Eqs. (66), or by considering the opportune variational statement and constitutive equations where the thermal and/or electrical contributions are discarded.

8 Results

The shells analyzed are simply supported one-layered or multilayered structures subjected to mechanical and field loads in harmonic form. First, three assessments are given which allows the refined models to be validated for the cases of applied mechanical load, imposed electric potential on the surfaces and imposed over-temperature on the surfaces. The refined models based on CUF theory are compared with well-known 3D and quasi-3D results given in the open literature [5, 15]. After this preliminary validation, a new benchmark is proposed to remark the importance of refined models with respect to classical ones and to evaluate the effects of multifield couplings. The benchmark considers three different loading cases in analogy with the preliminary assessments.

8.1 Assessments

The simply supported shell has radii of curvature $R_\alpha = 10$ m and $R_\beta = \infty$, the dimensions are $a = \frac{\pi}{3} R_\alpha = 10.471975512$ m and $b = 1$ m. The thickness ratios $s = R_\alpha / h$ investigated are equal to 2, 4, 6, 10, 20, 100 and 500 with total thickness h equals 5 m, 2.5 m, 1 m, 1.666667 m, 0.5 m, 0.1 m and 0.02 m, respectively. In the first assessment, a mechanical load is applied at the top surface in the z direction in the form $p_z = p_0 \sin(\frac{\pi \alpha}{a})$ with $p_0 = -1$ Pa and wave numbers $m = 1$ and $n = 0$. The shell has imposed electric potential $\Phi_t = \Phi_b = 0$ at the external surfaces. It is one-layered made where the piezoelectric PVDF material has Young modulus $E = 2$ GPa and Poisson ratio $\nu = 1/3$, piezoelectric coefficients $e_{31} = 0.0285\ \mathrm{C/m^2}$, $e_{32} = -0.0015\ \mathrm{C/m^2}$, $e_{33} = -0.051\ \mathrm{C/m^2}$ and $e_{15} = e_{24} = 0\ \mathrm{C/m^2}$ and dielectric constants $\varepsilon_{11} = \varepsilon_{22} = \varepsilon_{33} = 106.2 \times 10^{-12}\ \mathrm{C/V\,m}$. The three-dimensional solution is given by Dumir et al. [15] which consider a full electro-mechanical coupling. The refined models here given can also consider the thermal effect (with free conditions for the over-temperature at the external surfaces), in these cases the following properties must be given: specific heat per unit mass $C_v = 420\ \mathrm{J/kg\,K}$, coefficients of thermal expansion $\alpha_{11} = \alpha_{22} = \alpha_{33} = 0.9 \times 10^{-6}\ \mathrm{K^{-1}}$, thermal conductivity coefficients $\kappa_{11} = \kappa_{22} = \kappa_{33} = 2.1\ \mathrm{W/m\,K}$, pyroelectric constant $p_3 = 20 \times 10^{-6}\ \mathrm{C/m^2\,K}$ and mass density $\rho = 7600\ \mathrm{kg/m^3}$. Results are in non-dimensional form: $(\bar{u}, \bar{w}) = 100(u, w)E/hs^4|p_0|$, $\bar{\Phi} = d_0 E \Phi / hs^2|p_0|$ and $\bar{\mathcal{D}}_\alpha = \mathcal{D}_\alpha / d_0 s|p_0|$ with $d_0 = 30 \times 10^{-12}\ \mathrm{CN^{-2}}$; they are evaluated at different positions through the thickness. Table 1 compares the 3D solution by Dumir et al. [15] with refined LW models with

Table 1 First assessment: mechanical load applied to a PVDF piezoelectric shell. Comparison between refined and three-dimensional models for several thickness ratios R_α/h. The non-dimensional values are the maximum amplitudes in the plane

R_α/h	2	4	6	10	20	100	500
			$\bar{w}(0)$				
3D [15]	−31.47	−21.10	−18.96	−17.68	−16.98	−16.55	−16.48
LD4(u,Φ,θ)	−31.45	−21.10	−18.96	−17.68	−16.98	−16.55	−16.48
LD4(u,Φ)	−31.45	−21.10	−18.96	−17.68	−16.98	−16.55	−16.48
LD4(u,θ)	−31.60	−21.30	−19.16	−17.89	−17.18	−16.75	−16.68
LD4(u)	−31.60	−21.30	−19.16	−17.89	−17.18	−16.75	−16.68
			$\bar{u}(h/2)$				
3D [15]	2.046	−0.8806	−2.331	−3.572	−4.528	−5.297	−5.451
LD4(u,Φ,θ)	2.045	−0.8806	−2.331	−3.572	−4.528	−5.297	−5.451
LD4(u,Φ)	2.045	−0.8806	−2.331	−3.572	−4.528	−5.297	−5.451
LD4(u,θ)	2.102	−0.8775	−2.352	−3.613	−4.582	−5.361	−5.517
LD4(u)	2.102	−0.8775	−2.352	−3.613	−4.582	−5.361	−5.517
			$10^3\bar{\Phi}(0)$				
3D [15]	1.734	2.443	2.541	2.560	2.540	2.504	2.494
LD4(u,Φ,θ)	1.729	2.443	2.541	2.561	2.541	2.504	2.495
LD4(u,Φ)	1.729	2.442	2.540	2.560	2.540	2.503	2.494
LD4(u,θ)	–	–	–	–	–	–	–
LD4(u)	–	–	–	–	–	–	–
			$\bar{\mathcal{D}}_\alpha(0)$				
3D [15]	−0.3070	−0.4324	−0.4497	−0.4531	−0.4496	−0.4431	−0.4415
LD4(u,Φ,θ)	−0.3060	−0.4324	−0.4498	−0.4532	−0.4497	−0.4432	−0.4416
LD4(u,Φ)	−0.3060	−0.4323	−0.4497	−0.4531	−0.4496	−0.4431	−0.4415
LD4(u,θ)	–	–	–	–	–	–	–
LD4(u)	–	–	–	–	–	–	–

fourth order of expansion through the thickness for each modelled thermo-electro-mechanical variable, the "a priori" modelled variables are indicated in parentheses and in this way the couplings between the involved physical fields are clearly shown. LD4(u,Φ) model is an electro-mechanical model and it gives the 3D solution [15] for each thickness ratio R_α/h and for each variable proposed (transverse displacement $\bar{w}$, electric potential $\bar{\Phi}$ and in-plane electric displacement $\bar{\mathcal{D}}_\alpha$ in the middle of the shell, and in-plane displacement $\bar{u}$ at the top of the structure). In the case of thermo-electro-mechanical coupling, the LD4(u,Φ,θ) model gives the same LD4(u,Φ) results because the thermal field effects are not important in such a problem and they can be discarded. The importance of the electric field is clearly shown by means of LD4(u,θ) and LD4(u) models, when the electric potential is discarded a bigger transverse displacement is obtained because a part of the applied mechanical load is not converted in electrical work. The comparison between LD4(u,θ) and LD4(u) models also confirms the no importance of the thermal field. A further limitation of LD4(u,θ) and LD4(u) models is that they do not give any information about the electrical variables such as the electric potential and the electric displacements.

The simply supported shell has the same geometry, boundary conditions and material properties of the shell considered in the first assessment. In this second case an electric potential is applied on the external surfaces: $\Phi_t = 1$ V at the top and $\Phi_b = 0$ V at the bottom in sinusoidal form with wave numbers $m = 1$ and $n = 0$. The three-dimensional solution is given by Dumir et al. [15] for the full electro-mechanical

Table 2 Second assessment: electric potential applied to a PVDF piezoelectric shell. Comparison between refined and three-dimensional models for several thickness ratios R_α/h. The non-dimensional values are the maximum amplitudes in the plane

R_α/h	2	4	6	10	20	100	500
			$\bar{w}(0)$				
3D [15]	17.96	11.90	8.955	6.340	4.253	2.523	2.171
LD4(u,Φ,θ)	17.94	11.90	8.959	6.342	4.256	2.525	2.173
LD4(u,Φ)	17.94	11.90	8.955	6.340	4.253	2.523	2.172
			$\bar{u}(h/2)$				
3D [15]	−35.98	−28.74	−27.27	−26.49	−26.13	−25.99	−25.98
LD4(u,Φ,θ)	−35.98	−28.74	−27.26	−26.48	−26.13	−25.99	−25.97
LD4(u,Φ)	−35.98	−28.74	−27.27	−26.49	−26.13	−25.99	−25.98
			$\bar{\Phi}(0)$				
3D [15]	−0.4433	−0.4978	−0.5057	−0.5070	−0.5049	−0.5012	−0.5002
LD4(u,Φ,θ)	−0.4433	−0.4978	−0.5057	−0.5070	−0.5049	−0.5012	−0.5002
LD4(u,Φ)	−0.4433	−0.4978	−0.5057	−0.5070	−0.5049	−0.5012	−0.5002
			$\bar{\mathcal{D}}_\alpha(h/2)$				
3D [15]	141.6	157.3	163.4	168.6	172.7	176.1	176.8
LD4(u,Φ,θ)	177.0	177.0	177.0	177.0	177.0	177.0	177.0
LD4(u,Φ)	177.0	177.0	177.0	177.0	177.0	177.0	177.0

coupling, free conditions for the sovra-temperature are considered when the thermal effect is included in CUF refined models. Results are in no-dimensional form: $(\bar{u},\bar{w}) = 100(u,w)/d_0 s\Phi_0$, $\bar{\Phi} = \Phi/\Phi_0$ and $\bar{\mathcal{D}}_\alpha = hs\mathcal{D}_\alpha/d_0^2 E\Phi_0$ with $d_0 = 30\times10^{-12}$ CN^{-2} and $\Phi_0 = -1$ V; they are evaluated at different positions through the thickness. Table 2 compares the transverse displacement and the electric potential in the middle of the shell and in-plane mechanical and electrical displacements at the top of the structure for several thickness ratios R_α/h. LD4(u,Φ) is a refined electro-mechanical model which gives a quasi-3D description of the problem for each thickness value and variable analyzed (see the comparison with the 3D electro-mechanical solution by Dumir et al. [15]). Some problems are exhibited for the electric displacement because it is evaluated at the top of the structure where the electric potential is imposed ($\Phi_t = 1$ V), however in the results proposed in the next section it is clearly demonstrated how CUF refined models give a quasi-3D description of each electric displacement component through the thickness z. The comparison between LD4(u,Φ,θ) and LD4(u,Φ) models demonstrates how the thermal field effect can be discarded in such a problem, in particular for these two preliminary assessments where only one piezoelectric layer is embedded in the investigated structure.

The third assessment considers a two-layered shell, it is simply supported with the same geometry of the first two assessments. The investigated thickness ratios $s = R_\alpha/h$ are 10, 50, 100, 1000 which mean total thickness h equals 1 m, 0.2 m, 0.1 m, 0.01 m, respectively. An over-temperature in sinusoidal form (wave numbers $m = n = 1$) is imposed at the external surfaces: $\theta_t = 1$ K at the top and $\theta_b = 0$ K at the bottom. No piezoelectric layers are embedded in the shell, the bottom layer ($h_1 = 0.5h$) is in aluminium alloy Al2024 and the top layer ($h_2 = 0.5h$) is in titanium alloy Ti22. The Al2024 has Young modulus $E = 73$ GPa, Poisson ratio $\nu = 0.3$, mass density $\rho = 2800$ kg/m^3, specific heat per unit mass $C_v = 897$ J/kg K, coefficient of thermal expansion $\alpha = 25\times10^{-6}$ K^{-1} and thermal conductivity coefficient $\kappa = 130$ W/mK. The properties of the Ti22 are $E = 110$ GPa, $\nu = 0.32$, $\rho = 4420$ kg/m^3, $C_v = 560$ J/kg K, $\alpha = 8.6\times10^{-6}$ K^{-1} and $\kappa = 21.9$ W/mK. The quasi three-dimensional solution, in term of transverse displacement w in the middle of the thickness, has already been proposed in [5] for the validation of the coupled thermo-mechanical models, the reference solution is a typical thermal stress analysis where the temperature profile is "a priori" calculated by solving the Fourier heat conduction equation in order to give an opportune value of the thermal load.

Table 3 Third assessment: temperature imposed in a multilayered shell. Comparison between refined theories and a quasi three-dimensional model (thermal stress analysis) for several thickness ratios R_α/h. The dimensional values are the maximum amplitudes in the plane

R_α/h	10	50	100	1000
		$w(0)$ [mm]		
Ref. [5]	0.0010	0.0061	0.0129	0.0424
LD4(u,Φ,θ)	0.0010	0.0060	0.0129	0.0424
LD4(u,θ)	0.0010	0.0060	0.0129	0.0424

In Table 3, both LD4(u,Φ,θ) and LD4(u,θ) models give the reference solution because the two models are coincident, no electric field is included by the thermal load and by the elastic Al2024 and Ti22 layers. However, the LD4(u,Φ,θ) has preliminary been validated and then it can be used with confidence for those thermal analyses where the importance of the electric field is fundamental (see the benchmark proposed in the next section).

8.2 Thermo-electro-mechanical analysis of smart shells

The multilayered smart shell employed for the benchmarks proposed in this section is a simply supported shell with the same geometry of the assessment cases ($R_\alpha = 10$ m, $R_\beta = \infty$, $a = \frac{\pi}{3}R_\alpha = 10.471975512$ m and $b = 1$ m) with thickness ratios $s = R_\alpha/h = 20, 50, 100$ (which means total thickness h equals 0.5 m, 0.2 m and 0.1 m, respectively). The structure has four layers with lamination sequence PZT/0°/90°/PZT. The external layers are in PZT piezoelectric material with thickness values $h_1 = h_4 = 0.1h$, the internal layers are in graphite-epoxy material with thickness values $h_2 = h_3 = 0.4h$. The composite material has Young modulii $E_1 = 144.23$ GPa and $E_2 = E_3 = 9.65$ GPa, shear modulii $G_{12} = G_{13} = 4.14$ GPa and $G_{23} = 3.45$ GPa, Poisson ratios $\nu_{12} = \nu_{13} = \nu_{23} = 0.3$, mass density $\rho = 1389.23\,\mathrm{kg/m^3}$, specific heat per unit mass $C_v = 1409\,\mathrm{J/kg\,K}$, coefficients of thermal expansion $\alpha_{11} = 1.1 \times 10^{-6}\,\mathrm{K^{-1}}$ and $\alpha_{22} = \alpha_{33} = 25.2 \times 10^{-6}\,\mathrm{K^{-1}}$, thermal conductivity coefficients $\kappa_{11} = 4.48$ W/mK and $\kappa_{22} = \kappa_{33} = 3.21$ W/mK and dielectric constants $\varepsilon_{11} = 3.098966 \times 10^{-11}$ F/m and $\varepsilon_{22} = \varepsilon_{33} = 2.6562563 \times 10^{-11}$ F/m. The piezoelectric layer has Young modulus $E = 63$ GPa, Poisson ratio $\nu = 0.28$, mass density $\rho = 7600\,\mathrm{kg/m^3}$, specific heat per unit mass $C_v = 420\,\mathrm{J/kg\,K}$, coefficient of thermal expansion $\alpha = 0.9 \times 10^{-6}\,\mathrm{K^{-1}}$, thermal conductivity coefficient $\kappa = 2.1$ W/mK, pyroelectric constant $p_3 = 20 \times 10^{-6}\,\mathrm{C/m^2\,K}$, piezoelectric coefficients $e_{31} = e_{32} = -5.20\,\mathrm{C/m^2}$, $e_{33} = 15.08\,\mathrm{C/m^2}$ and $e_{15} = e_{24} = 12.72\,\mathrm{C/m^2}$ and dielectric constants $\varepsilon_{11} = \varepsilon_{22} = 15.3 \times 10^{-9}$ F/m and $\varepsilon_{33} = 15.0 \times 10^{-9}$ F/m. The shell proposed (see Fig. 1) can be subjected to three different loadings. The first case considers a bi-sinusoidal mechanical pressure applied at the top surface with amplitude $p_0 = 1$ Pa and wave numbers $m = n = 1$, the electric potential is set to zero at both top and bottom surfaces ($\Phi_t = \Phi_b = 0$) and the over-temperature is free. The second case considers a bi-sinusoidal electric voltage applied at the top of the shell with amplitude $\Phi_t = 1$ V and wave numbers $m = n = 1$, the bottom is set to zero ($\Phi_b = 0$ V), the over-temperature is free at both top and bottom surfaces. The third case analyzes a shell with imposed bi-sinusoidal over-temperature at the top surface with amplitude $\theta_t = 1$ K and wave numbers $m = n = 1$. The bottom surface has a zero imposed over-temperature, the electric potential is free considered at both the top and bottom of the shell.

Table 4 proposes the results for the shell subjected to the mechanical load (sensor configuration). The results given by the LD4(u,Φ,θ) can be considered as a quasi-3D description as confirmed by Fig. 3 where transverse displacement, sovra-temperature, electric potential, transverse normal electric displacement, in-plane stress and transverse shear stress are evaluated through the thickness of the shell for the thickness ratio $R_\alpha/h = 50$. The LD4(u,Φ,θ) model gives a transverse displacement not constant through the thickness with different slopes between the layers, the bending generates an over-temperature profile with positive values for the compressed part and negative values for the enlarged part (however the effect is very small because the values of the over-temperature are in 10^{-8} K). The generated electric potential confirms the imposed zero values at the external surfaces, while the transverse normal electric displacement is discontinuous at the interfaces (this problem could be solved by modelling it a priori as already discussed in a previous author's work [7]). The sign of in-plane stress confirms the bending behavior and its discontinuity at the interfaces is a typical feature of such a variable. The transverse shear stress confirms the boundary loading conditions (zero $\sigma_{\beta z}$ at the external surfaces because the transverse pressure is applied at the

Table 4 Benchmark: mechanical load applied to a multilayered smart shell. Thermo-electro-mechanical variables evaluated by means of classical and refined two-dimensional models. The dimensional values are the maximum amplitudes in the plane

	$w(0)$ [10^{-9} m]	$\theta(0)$ [10^{-8} K]	$\Phi(0)$ [V]	$\sigma_{\alpha\alpha}(0.5h)$ [Pa]	$\mathcal{D}_z(0.45h)$ [10^{-10} C/m^2]
		$R_\alpha/h = 20$			
LD4(u, Φ, θ)	0.0714	−0.1839	0.0010	1.7592	0.5606
ED4(u, Φ, θ)	0.0672	−0.2495	0.0010	1.3788	0.8782
FSDT(u, Φ, θ)	0.0418	−0.0536	0.0007	1.4456	1.1686
CLT(u, Φ, θ)	0.0161	−0.0001	0.0005	0.9717	0.0706
LD4(u, Φ)	0.0714	–	0.0010	1.7595	0.5608
LD4(u, θ)	0.0727	−0.1822	–	1.4454	–
LD4(u)	0.0728	–	–	2.1152	–
		$R_\alpha/h = 50$			
LD4(u, Φ, θ)	0.3955	−0.0996	0.0027	5.4081	2.1279
ED4(u, Φ, θ)	0.3876	−0.1381	0.0027	5.0383	2.3792
FSDT(u, Φ, θ)	0.3049	0.0892	0.0016	6.4163	2.3861
CLT(u, Φ, θ)	0.2434	0.0091	0.0015	5.7853	1.2436
LD4(u, Φ)	0.3955	–	0.0027	5.4082	2.1882
LD4(u, θ)	0.4119	−0.0891	–	4.0316	–
LD4(u)	0.4119	–	–	7.3353	–
		$R_\alpha/h = 100$			
LD4(u, Φ, θ)	2.1270	0.0228	0.0052	16.248	11.059
ED4(u, Φ, θ)	2.1141	0.0536	0.0052	15.974	11.259
FSDT(u, Φ, θ)	1.8930	0.2893	0.0028	21.279	10.520
CLT(u, Φ, θ)	1.7911	0.0335	0.0028	20.592	9.2622
LD4(u, Φ)	2.1271	–	0.0052	16.248	11.060
LD4(u, θ)	2.2310	0.0422	–	10.876	–
LD4(u)	2.2311	–	–	28.721	–

top of the shell in the same direction of the σ_{zz} stress). An important feature of Table 4 is the comparison between several thermo-electro-mechanical models, refined LW and ESL models are compared with the classical ones (FSDT(u, Φ, θ) and CLT(u, Φ, θ)). For thick shell the use of the LD4(u, Φ, θ) is mandatory for each evaluated variable, the ED4(u, Φ, θ) model gives quite good results for thin shells even if it exhibits some problems for the evaluation of stresses and over-temperature. Classical theories are always inadequate for each thickness ratio and for each considered variable, in particular CLT(u, Φ, θ) gives very wrong results. LD4(u, Φ), LD4(u, θ) and LD4(u) models allow the evaluation of the multifield effects by using a fourth order of expansion for the modelled variables in LW form. It is clear how the thermal effect can be discarded while the electric effect is fundamental, for example when the electric effect is discarded (as in LD4(u, θ) and LD4(u)) bigger transverse displacement values are obtained because a part of the mechanical load work is not converted in electric work (typical piezoelectric effect). When a physical field is discarded some variables cannot be evaluated, LD4(u, Φ) does not allow the over-temperature evaluation, LD4(u, θ) does not allow the electric potential and the electric displacements evaluations, LD4(u) only allows the evaluation of the mechanical variables. The multifield effects are almost independent on the thickness ratio.

Table 5 proposes the results for the shell when the electric potential is imposed at the external surfaces (actuator configuration). In the case of thermo-electro-mechanical coupling the LD4(u, Φ, θ) gives a quasi-3D description for each thickness ratio and variable in-

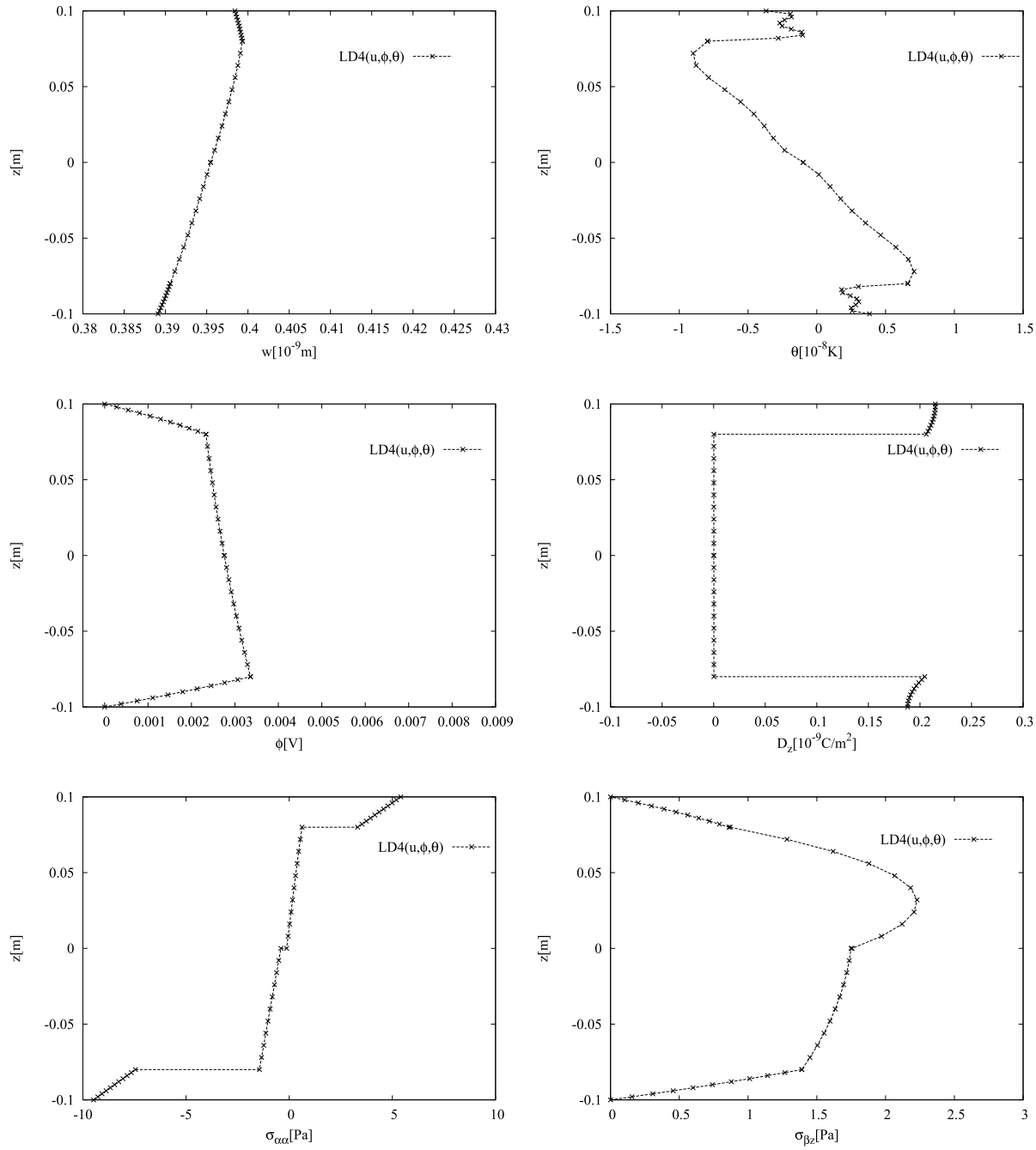

Fig. 3 Benchmark: mechanical load applied to a moderately thin ($R_\alpha/h = 50$) smart shell. Thermo-electro-mechanical variables through the thickness z via LD4(u, Φ, θ) model

vestigated, the ESL approach (ED4(u, Φ, θ)) exhibits big difficulties for each thickness ratio while classical theories are completely inadequate. The physical field effects can be evaluated by means of the LD4(u, Φ) model, further models cannot be considered (i.e., LD4(u, θ) and LD4(u) ones) because they do not allow the electric potential to be imposed. LD4(u, Φ) results demonstrate as the thermal field ef-

Table 5 Benchmark: electric potential applied to a multilayered smart shell. Thermo-electro-mechanical variables evaluated by means of classical and refined two-dimensional models. The dimensional values are the maximum amplitudes in the plane

	$w(0)$ [10^{-9} m]	$\theta(0)$ [10^{-9} K]	$\Phi(0)$ [V]	$\sigma_{\alpha\alpha}(0.5h)$ [Pa]	$\mathcal{D}_z(0.45h)$ [10^{-8} C/m^2]
		$R_\alpha/h = 20$			
LD4(u, Φ, θ)	−0.0131	0.3751	0.4134	−1.0722	−0.5458
ED4(u, Φ, θ)	−0.0377	−0.6141	0.4142	1.2230	−0.5079
FSDT(u, Φ, θ)	−0.1598	6.1683	0.4094	−3.7710	−0.4547
CLT(u, Φ, θ)	0.0017	0.1001	0.4108	−1.1715	−0.3868
LD4(u, Φ)	−0.0131	–	0.4134	−1.0722	−0.5458
		$R_\alpha/h = 50$			
LD4(u, Φ, θ)	−0.0091	0.0786	0.4854	−0.3695	−0.2354
ED4(u, Φ, θ)	−0.0267	−0.3261	0.4855	0.6534	−0.2214
FSDT(u, Φ, θ)	−0.1560	−3.0744	0.4851	−1.4140	−0.1988
CLT(u, Φ, θ)	0.0017	0.0367	0.4853	−0.5168	−0.1698
LD4(u, Φ)	−0.0091	–	0.4854	−0.3695	−0.2354
		$R_\alpha/h = 100$			
LD4(u, Φ, θ)	−0.0078	0.0323	0.4968	−0.3018	−0.1430
ED4(u, Φ, θ)	−0.0230	−0.1736	0.4968	0.2250	−0.1364
FSDT(u, Φ, θ)	−0.1412	1.9452	0.4967	−0.5517	−0.1274
CLT(u, Φ, θ)	0.0017	0.0122	0.4968	−0.3380	−0.1098
LD4(u, Φ)	−0.0078	–	0.4968	−0.3018	−0.1430

fect can be discarded for such a problem because it is very small, this fact is confirmed by the small values of the over-temperature (order of $10^{-9}K$). In Fig. 4, it is clearly shown as the LD4(u, Φ, θ) model gives a quasi-3D description of the problem in terms of different physical variables. The electric potential is clearly imposed and calculated ($\Phi_t = 1$ V and $\Phi_b = 0$ V), it generates a transverse displacement with a zigzag form because the shell has different layers, such a displacement generates a temperature profile in accordance with the bending behavior (but the temperature values are very small). The transverse normal electric displacement is better evaluated if compared with the sensor case and the in-plane stress confirms the bending behavior with a typical discontinuity at the interfaces, finally the transverse shear stress is correctly plotted and it satisfies the boundary loading conditions.

The case of smart shell with imposed over-temperature at the external surfaces is analyzed in Table 6 and in Fig. 5. Figure 5 clearly shows a quasi-3D description of the smart shell behavior via the LD4(u, Φ, θ) model, the over-temperature is imposed equal to 1 K at the top and $0\,K$ at the bottom, and the model is able to calculate the temperature profile, such a temperature profile generates a bending as indicated by the transverse displacement evaluation (typical zigzag form which is shown because an LW model is employed for a multilayered structure). An electric potential is generated by this bending and no boundary conditions are imposed. The transverse normal electric displacement shows a discontinuity at the interfaces as in the first benchmark [7]. The in-plane and transverse shear stresses confirm the bending behavior and the correct boundary loading conditions. The LD4(u, Φ, θ) model proposed in Table 6 gives a correct description of the problem for each thickness ratio and for each variable investigated. Refined ESL and classical models are completely inadequate for each thickness ratio and for each variable evaluated. Thermo-mechanical models are the only two- and one-field models applicable to this benchmark because we need to modelling the temperature field in order to impose it at the external surfaces. The LD4(u, θ) model demonstrates the importance of the electric field for such a problem, in fact the electric potential modelling

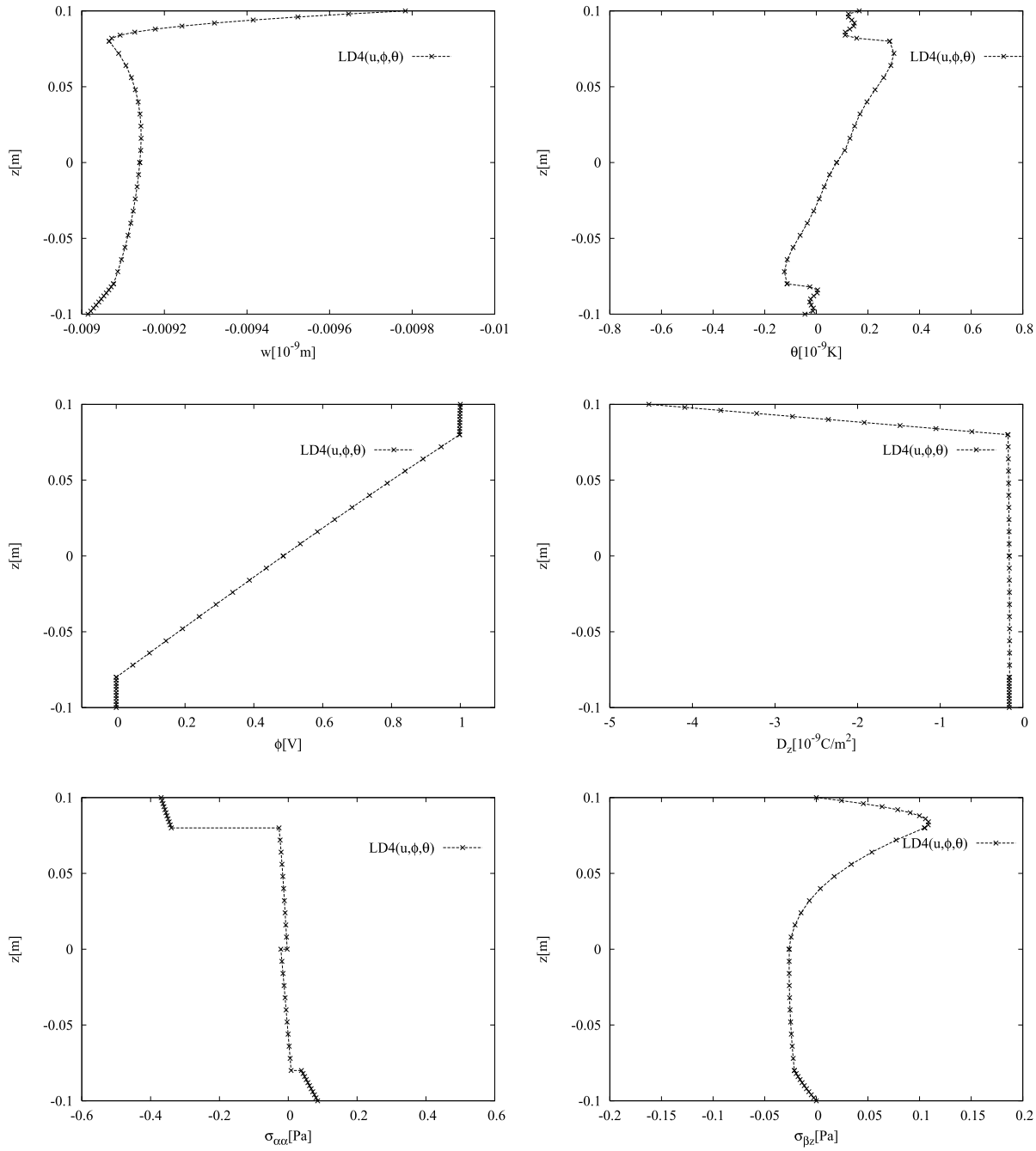

Fig. 4 Benchmark: electric potential applied to a moderately thin ($R_\alpha/h = 50$) smart shell. Thermo-electro-mechanical variables through the thickness z via LD4(u, Φ, θ) model

must always be included to avoid uncorrect results. The electrical effect cannot be discarded in this last example.

9 Conclusions

One-layered and multilayered simply supported smart shells with constant radii of curvature and embed-

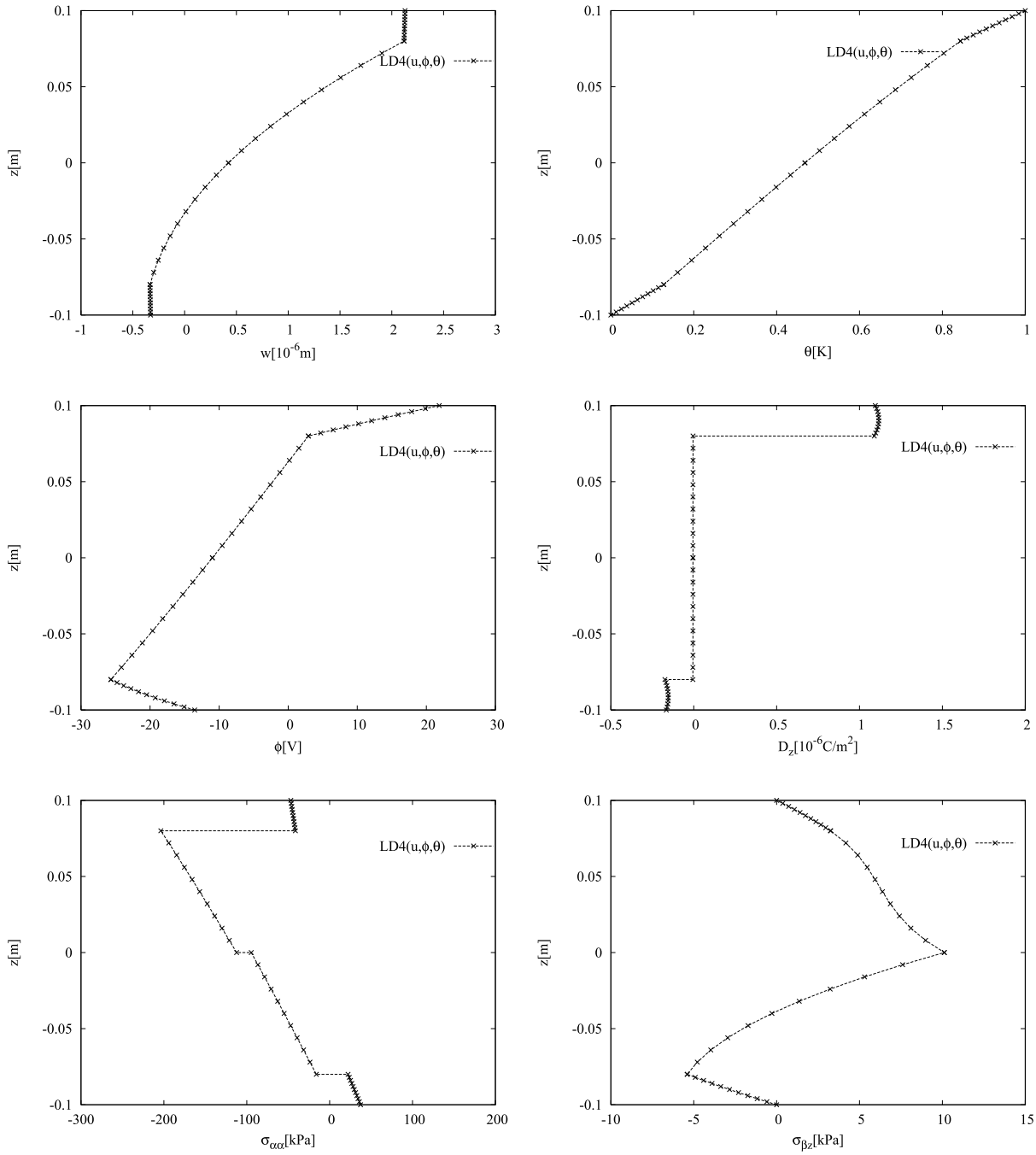

Fig. 5 Benchmark: temperature imposed to a moderately thin ($R_\alpha / h = 50$) smart shell. Thermo-electro-mechanical variables through the thickness z via LD4(u, Φ, θ) model

Table 6 Benchmark: temperature imposed to a multilayered smart shell. Thermo-electro-mechanical variables evaluated by means of classical and refined two-dimensional models. The dimensional values are the maximum amplitudes in the plane

	$w(0)$ [10^{-6} m]	$\theta(0)$ [K]	$\Phi(0)$ [V]	$\sigma_{\alpha\alpha}(0.5h)$ [Pa]	$\mathcal{D}_z(0.45h)$ [10^{-6} C/m^2]
			$R_\alpha/h = 20$		
LD4(u, Φ, θ)	−0.1078	0.3402	−12.305	−19551	1.8496
ED4(u, Φ, θ)	−0.0126	0.3402	−60.326	−135740	2.6067
FSDT(u, Φ, θ)	0.3266	0.3349	34.961	19371	0.5606
CLT(u, Φ, θ)	0.2400	0.3349	−17.821	12132	0.4894
LD4(u, θ)	−0.1412	0.3402	–	−17764	–
			$R_\alpha/h = 50$		
LD4(u, Φ, θ)	0.4232	0.4683	−10.968	−46862	1.1161
ED4(u, Φ, θ)	0.5058	0.4683	−38.983	−191340	1.2050
FSDT(u, Φ, θ)	0.8988	0.4681	61.818	64606	0.6456
CLT(u, Φ, θ)	0.7847	0.4681	−8.5870	54308	0.5714
LD4(u, θ)	0.3383	0.4683	–	−36893	–
			$R_\alpha/h = 100$		
LD4(u, Φ, θ)	1.5477	0.4924	−2.5204	−49534	1.2604
ED4(u, Φ, θ)	1.6522	0.4924	−14.815	−198070	1.2997
FSDT(u, Φ, θ)	2.4110	0.4924	61.826	79358	1.3293
CLT(u, Φ, θ)	2.3114	0.4924	−3.7329	69196	1.2709
LD4(u, θ)	1.4273	0.4924	–	−38823	–

ded piezoelectric layers have been analyzed in this paper in the case of applied mechanical load, imposed electric voltage on the external surfaces or imposed over-temperature values at the top and bottom of the structures. Refined multifield two-dimensional models have been proposed in the framework of a full coupling between electrical, mechanical and thermal fields, these models have been developed in both Equivalent Single Layer (ESL) or Layer Wise (LW) form. Refined LW models give a quasi-3D description in terms of each mechanical, thermal and electrical variable, while classical models (those based on Kirchhoff or Reissner/Mindlin hypotheses) are completely inadequate for such problems. Refined ESL models are suitable only for some particular cases. LW refined thermo-electro-mechanical models are mandatory for the investigation of the static response of multilayered piezoelectric shells when subjected to mechanical or field loadings, and they also allow the different multifield coupling effects to be evaluated. These multifield effects do not depend on the thickness of the structure considered and they do not depend on the curvature (in the case of shell geometries).

Appendix: Explicit form of fundamental nuclei

Fundamental nucleus $\boldsymbol{K}_{uu}^{k\tau s}$, of (3×3) dimension, is the same for each loading case:

$$K_{uu_{11}} = Q_{55}^k J_{\underset{\alpha}{\beta}}^{k\tau s} \frac{1}{R_\alpha^{k\,2}} - Q_{55}^k J_\beta^{k\tau_z s} \frac{1}{R_\alpha^k} - Q_{55}^k J_\beta^{k\tau s_z} \frac{1}{R_\alpha^k} + Q_{55}^k J_{\alpha\beta}^{k\tau_z s_z} + Q_{11}^k J_{\underset{\alpha}{\beta}}^{k\tau s} \bar{\alpha}^2 + Q_{66}^k J_{\underset{\beta}{\alpha}}^{k\tau s} \bar{\beta}^2,$$

$$K_{uu_{12}} = J^{k\tau s} \bar{\alpha}\bar{\beta}\left(Q_{12}^k + Q_{66}^k\right) = K_{uu_{21}},$$

$$K_{uu_{13}} = -\frac{1}{R_\alpha^k} Q_{11}^k J_{\underset{\alpha}{\beta}}^{k\tau s} \bar{\alpha} - \frac{1}{R_\beta^k} Q_{12}^k J^{k\tau s} \bar{\alpha} - \frac{1}{R_\alpha^k} Q_{55}^k J_{\underset{\alpha}{\beta}}^{k\tau s} \bar{\alpha} + Q_{55}^k J^{k\tau_z s} \bar{\alpha} - Q_{13}^k J^{k\tau s_z} \bar{\alpha},$$

$$
\begin{aligned}
K_{uu_{22}} &= \frac{1}{R_\beta^{k\,2}} Q_{44}^k J_{\frac{\alpha}{\beta}}^{k\tau s} - \frac{1}{R_\beta^k} Q_{44}^k J_\alpha^{k\tau_z s} - \frac{1}{R_\beta^k} Q_{44}^k J_\alpha^{k\tau s_z} + Q_{44}^k J_{\alpha\beta}^{k\tau_z s_z} + Q_{22}^k J_{\frac{\alpha}{\beta}}^{k\tau s} \bar{\beta}^2 + Q_{66}^k J_{\frac{\beta}{\alpha}}^{k\tau s} \bar{\alpha}^2,\\
K_{uu_{23}} &= -Q_{12}^k J^{k\tau s} \bar{\beta} \frac{1}{R_\alpha^k} - Q_{22}^k J_{\frac{\alpha}{\beta}}^{k\tau s} \bar{\beta} \frac{1}{R_\beta^k} + Q_{44}^k J_\alpha^{k\tau_z s} \bar{\beta} - Q_{23}^k J_\alpha^{k\tau s_z} \bar{\beta} - Q_{44}^k J_{\frac{\alpha}{\beta}}^{k\tau s} \frac{1}{R_\beta^k} \bar{\beta},\\
K_{uu_{31}} &= Q_{55}^k J_\beta^{k\tau s_z} \bar{\alpha} - Q_{13}^k J_\beta^{k\tau_z s} \bar{\alpha} - Q_{11}^k J_{\frac{\beta}{\alpha}}^{k\tau s} \bar{\alpha} \frac{1}{R_\alpha^k} - Q_{12}^k J^{k\tau s} \bar{\alpha} \frac{1}{R_\beta^k} - Q_{55}^k J_{\frac{\beta}{\alpha}}^{k\tau s} \bar{\alpha} \frac{1}{R_\alpha^k},\\
K_{uu_{32}} &= Q_{44}^k J_\alpha^{k\tau s_z} \bar{\beta} - Q_{23}^k J_\alpha^{k\tau_z s} \bar{\beta} - Q_{12}^k J^{k\tau s} \bar{\beta} \frac{1}{R_\alpha^k} - Q_{22}^k J_{\frac{\alpha}{\beta}}^{k\tau s} \bar{\beta} \frac{1}{R_\beta^k} - Q_{44}^k J_{\frac{\alpha}{\beta}}^{k\tau s} \bar{\beta} \frac{1}{R_\beta^k},\\
K_{uu_{33}} &= Q_{55}^k J_{\frac{\beta}{\alpha}}^{k\tau s} \bar{\alpha}^2 + Q_{44}^k J_{\frac{\alpha}{\beta}}^{k\tau s} \bar{\beta}^2 + Q_{33}^k J_{\alpha\beta}^{k\tau_z s_z} + Q_{11}^k J_{\frac{\beta}{\alpha}}^{k\tau s} \frac{1}{R_\alpha^{k\,2}} + Q_{12}^k J^{k\tau s} \frac{2}{R_\alpha^k R_\beta^k}\\
&\quad + Q_{22}^k J_{\frac{\alpha}{\beta}}^{k\tau s} \frac{1}{R_\beta^{k\,2}} + Q_{13}^k J_\beta^{k\tau_z s} \frac{1}{R_\alpha^k} + Q_{23}^k J_\alpha^{k\tau_z s} \frac{1}{R_\beta^k} + Q_{13}^k J_\beta^{k\tau s_z} \frac{1}{R_\alpha^k} + Q_{23}^k J_\alpha^{k\tau s_z} \frac{1}{R_\beta^k}.
\end{aligned} \tag{1}
$$

Fundamental nucleus $\boldsymbol{K}_{u\Phi}^{k\tau s}$, of (3×1) dimension, is in common for each considered case:

$$
\begin{aligned}
K_{u\Phi_{11}} &= \bar{\alpha} J_\beta^{k\tau_z s} e_{15}^k - \bar{\alpha} J_\beta^{k\tau s_z} e_{31}^k - \bar{\alpha} \frac{1}{R_\alpha^k} J_{\frac{\beta}{\alpha}}^{k\tau s} e_{15}^k,\\
K_{u\Phi_{21}} &= \bar{\beta} J_\alpha^{k\tau_z s} e_{24}^k - \bar{\beta} J_\alpha^{k\tau s_z} e_{32}^k - \bar{\beta} \frac{1}{R_\beta^k} J_{\frac{\alpha}{\beta}}^{k\tau s} e_{24}^k,\\
K_{u\Phi_{31}} &= \bar{\alpha}^2 J_{\frac{\beta}{\alpha}}^{k\tau s} e_{15}^k + J_{\alpha\beta}^{k\tau_z s_z} e_{33}^k + \bar{\beta}^2 J_{\frac{\alpha}{\beta}}^{k\tau s} e_{24}^k\\
&\quad + \frac{1}{R_\alpha^k} J_\beta^{k\tau s_z} e_{31}^k + \frac{1}{R_\beta^k} J_\alpha^{k\tau s_z} e_{32}^k.
\end{aligned} \tag{2}
$$

Fundamental nucleus $\boldsymbol{K}_{u\theta}^{k\tau s}$, of (3×1) dimension, is the same for each considered case:

$$
\begin{aligned}
K_{u\theta_{11}} &= \bar{\alpha} J_\beta^{k\tau s} \lambda_1^k, \qquad K_{u\theta_{21}} = \bar{\beta} J_\alpha^{k\tau s} \lambda_2^k,\\
K_{u\theta_{31}} &= -\frac{1}{R_\alpha^k} J_\beta^{k\tau s} \lambda_1^k - \frac{1}{R_\beta^k} J_\alpha^{k\tau s} \lambda_2^k - J_{\alpha\beta}^{k\tau_z s} \lambda_3^k.
\end{aligned} \tag{3}
$$

Fundamental nucleus $\boldsymbol{K}_{\Phi u}^{k\tau s}$, of (1×3) dimension, does not change for each load case:

$$
\begin{aligned}
K_{\Phi u_{11}} &= -\bar{\alpha} J_{\frac{\beta}{\alpha}}^{k\tau s} e_{15}^k \frac{1}{R_\alpha^k} + \bar{\alpha} J^{k\tau s_z} e_{15}^k - \bar{\alpha} J^{k\tau_z s} e_{31}^k,\\
K_{\Phi u_{12}} &= -\bar{\beta} J_{\frac{\alpha}{\beta}}^{k\tau s} e_{24}^k \frac{1}{R_\beta^k} + \bar{\beta} J_\alpha^{k\tau s_z} e_{24}^k - \bar{\beta} J_\alpha^{k\tau_z s} e_{32}^k,\\
K_{\Phi u_{13}} &= \bar{\alpha}^2 J_{\frac{\beta}{\alpha}}^{k\tau s} e_{15}^k + J_{\alpha\beta}^{k\tau_z s_z} e_{33}^k\\
&\quad + \bar{\beta}^2 J_{\frac{\alpha}{\beta}}^{k\tau s} e_{24}^k + J_\beta^{k\tau_z s} e_{31}^k \frac{1}{R_\alpha^k} + J_\alpha^{k\tau_z s} e_{32}^k \frac{1}{R_\beta^k}.
\end{aligned} \tag{4}
$$

Fundamental nucleus $\boldsymbol{K}_{\Phi\Phi}^{k\tau s}$, of (1×1) dimension, is in common for each considered case:

$$
K_{\Phi\Phi_{11}} = -\bar{\alpha}^2 J_{\frac{\beta}{\alpha}}^{k\tau s} \varepsilon_{11}^k - J_{\alpha\beta}^{k\tau_z s_z} \varepsilon_{33}^k - \bar{\beta}^2 J_{\frac{\alpha}{\beta}}^{k\tau s} \varepsilon_{22}^k. \tag{5}
$$

Fundamental nucleus $\boldsymbol{K}_{\Phi\theta}^{k\tau s}$, of (1×1) dimension, is in common for each multifield problem:

$$
K_{\Phi\theta_{11}} = J_{\alpha\beta}^{k\tau_z s} p_3^k. \tag{6}
$$

Fundamental nucleus $\boldsymbol{K}_{\theta u}^{k\tau s}$ (of (1×3) dimension) for the cases of applied mechanical load or imposed electric potential is:

$$
\begin{aligned}
K_{\theta u_{11}} &= \bar{\alpha} J_\beta^{k\tau s} \lambda_1^k, \qquad K_{\theta u_{12}} = \bar{\beta} J_\alpha^{k\tau s} \lambda_2^k,\\
K_{\theta u_{13}} &= -J_{\alpha\beta}^{k\tau s_z} \lambda_3^k - J_\beta^{k\tau s} \lambda_1^k \frac{1}{R_\alpha^k} - J_\alpha^{k\tau s} \lambda_2^k \frac{1}{R_\beta^k}.
\end{aligned} \tag{7}
$$

The same nucleus for the case of imposed temperature has zero components:

$$
K_{\theta u_{11}} = K_{\theta u_{12}} = K_{\theta u_{13}} = 0. \tag{8}
$$

Fundamental nucleus $\boldsymbol{K}_{\theta\Phi}^{k\tau s}$, of (1×1) dimension, for the case of applied mechanical load or imposed electric potential is:

$$
K_{\theta\Phi_{11}} = J_{\alpha\beta}^{k\tau s_z} p_3^k. \tag{9}
$$

The same nucleus for the case of imposed temperature has zero components:

$$
K_{\theta\Phi_{11}} = 0. \tag{10}
$$

Fundamental nucleus $\boldsymbol{K}_{\theta\theta}^{k\tau s}$, of (1×1) dimension, for the case of applied mechanical load or imposed electric potential is:

$$K_{\theta\theta_{11}} = -\chi^k J_{\alpha\beta}^{k\tau s}. \tag{11}$$

Fundamental nucleus $\boldsymbol{K}_{\theta\theta}^{k\tau s}$, of (1×1) dimension, for the case of imposed temperature is:

$$K_{\theta\theta_{11}} = -\bar{\alpha}^2 \kappa_{11}^k J_{\substack{\beta \\ \alpha}}^{k\tau s} - \bar{\beta}^2 \kappa_{22}^k J_{\substack{\alpha \\ \beta}}^{k\tau s} - \kappa_{33}^k J_{\alpha\beta}^{k\tau_z s_z}. \tag{12}$$

In each proposed fundamental nucleus we have the terms $\bar{\alpha} = m\pi/a$ and $\bar{\beta} = n\pi/b$, where m and n are the wave numbers in in-plane directions, and a and b are the shell dimensions.

References

1. Carrera E, Brischetto S, Nali P (2008) Variational statements and computational models for multifiled problems and multilayered structures. Mech Adv Mat Struct 15:182–198
2. Carrera E, Brischetto S, Nali P (2011) Plates and shells for smart structures: classical and advanced theories for modeling and analysis. Wiley, New Delhi
3. Brischetto S, Carrera E (2012) Coupled thermo-electro-mechanical analysis of smart plates embedding composite and piezoelectric layers. J Therm Stresses 35:766–804
4. Nowinski JL (1978) Theory of thermoelasticity with applications. Sijthoff & Noordhoff, The Netherlands
5. Brischetto S, Carrera E (2010) Coupled thermo-mechanical analysis of one-layered and multilayered isotropic and composite shells. Comput Model Eng Sci 56:249–301
6. Carrera E, Brischetto S, Cinefra M (2010) Variable kinematics and advanced variational statements for free vibrations analysis of piezoelectric plates and shells. Comput Model Eng Sci 65:259–342
7. Carrera E, Brischetto S (2007) Piezoelectric shell theories with "a priori" continuous transverse electro-mechanical variables. J Mech Mater Struct 2:377–399
8. Altay GA, Dökmeci MC (1996) Fundamental variational equations of discontinuous thermopiezoelectric fields. Int J Eng Sci 34:769–782
9. Altay GA, Dökmeci MC (1996) Some variational principles for linear coupled thermoelasticity. Int J Solids Struct 33:3937–3948
10. Cannarozzi AA, Ubertini F (2001) A mixed variational method for linear coupled thermoelastic analysis. Int J Solids Struct 38:717–739
11. Luo Q, Luo Z, Tong L (2011) A variational principle and finite element formulation for multi-physics PLZT ceramics. Mech Res Commun 38:198–202
12. Tauchert TR, Ashida F, Noda N, Adali S, Verijenko V (2000) Developments in thermopiezoelasticity with relevance to smart composite structures. Compos Struct 48:31–38
13. El-Karamany AS (2009) Uniqueness theorem and Hamilton's principle in linear micropolar thermopiezoelectric/piezomagnetic continuum with two relaxation times. Meccanica 44:19–47
14. Tong ZH, Lo SH, Jiang CP, Cheung YK (2008) An exact solution for the three-phase thermo-electro-magneto-elastic cylinder model and its application to piezoelectric-magnetic fiber composites. Int J Solids Struct 45:5205–5219
15. Dumir PC, Dube GB, Kapuria S (1997) Exact piezoelastic solution of simply supported orthotropic circular cylindrical panel in cylindrical bending. Int J Solids Struct 37:685–702
16. Dai HL, Wang X (2006) Magneto-thermo-electro-elastic transient response in a piezoelectric hollow cylinder subjected to complex loadings. Int J Solids Struct 43:5628–5646
17. Ganesan N, Kadoli R (2005) Semianalytical finite element analysis of piezothermoelastic shells of revolution. Comput Struct 83:1305–1319
18. Oh J, Cho M (2007) Higher order zig-zag theory for smart composite shells under mechanical-thermo-electric loading. Int J Solids Struct 44:100–127
19. Roy T, Manikandan P, Chakraborty D (2010) Improved shell finite element for piezothermoelastic analysis of smart fiber reinforced composite structures. Finite Elem Anal Des 46:710–720
20. Shariyat M (2008) Dynamic buckling of suddenly loaded imperfect hybrid FGM cylindrical shells with temperature-dependent material properties under thermo-electro-mechanical loads. Int J Mech Sci 50:1561–1571
21. Sheng GG, Wang X (2010) Response and control of functionally graded laminated piezoelectric shells under thermal shock and moving loadings. Compos Struct 93:132–141
22. Wu X-H, Shen Y-P, Chen C (2003) An exact solution for functionally graded piezothermoelastic cylindrical shell as sensors or actuators. Mater Lett 57:3532–3542
23. Kaminski M, Corigliano A (2012) Sensitivity, probabilistic and stochastic analysis of the thermo-piezoelectric phenomena in solids by the stochastic perturbation technique. Meccanica 47:877–891
24. Montanaro A (2011) On piezothermoelastic plates subject to prescribed boundary temperature. Meccanica 46:383–398
25. Abd-Alla AM, Mahmoud SR (2010) Magneto-thermo-elastic problem in rotating non-homogeneous orthotropic hollow cylinder under the hyperbolic heat conduction model. Meccanica 45:451–462
26. Kirchhoff G (1850) Über das dleichgewicht und die bewegung einer elastishen scheibe. J Reine Angew Math 40:51–88
27. Reissner E (1945) The effect of transverse shear deformation on the bending of elastic plates. J Appl Mech 12:69–77
28. Mindlin RD (1951) Influence of rotatory inertia and shear in flexural motions of isotropic elastic plates. J Appl Mech 18:31–38
29. Leissa AW (1969) Vibration of plates. NASA SP-160 Report, Washington, USA
30. Reddy JN (2004) Mechanics of laminated composite plates and shells. Theory and analysis. CRC Press, New York